Title: Prenatal Stress Dysregulates Resting-State Functional Connectivity and Sensory Motifs

Authors: Zahra Jafari[1,2,4], Zahra Rezaei[1,4], Navvab Afrashteh[1], Reza Torabi[1], Surjeet Singh[1], Bryan E. Kolb[1], Jörn Davidsen[3], Majid H. Mohajerani[1*]

[1]University of Lethbridge, Faculty of Arts and Sciences, Department of Neuroscience, 4401 University Dr. W., Lethbridge, Alberta, Canada, T1K 3M4.

[2]Department of Basic Sciences in Rehabilitation, School of Rehabilitation Sciences, Iran University of Medical Science (IUMS), Tehran, Iran

[3]Complexity Science Group, Department of Physics and Astronomy, Faculty of Science, University of Calgary, Calgary, AB, T2N 1N4, Canada.

[4]These authors contributed equally. The co-first authorship order determined by coin flip.

*Corresponding author: Majid H. Mohajerani

Department of Neuroscience, Canadian Centre for Behavioural Neuroscience, University of Lethbridge, Lethbridge, AB, Canada, T1K 3M4

Email: mohajerani@uleth.ca, Tel: 403 394 3950

Author Contribution: Conceptualization, M.H.M., Z.J., B.E.K.; Experimentation, M.H.M, Z.J, N.A.; Formal Analysis, Z.R.; Analysis advise, N.A., R.T., S.S., J.D.; Writing - Original Draft, Z.R., Z.J., M.H.M.; Writing - Review & Editing, Z.R., Z.J., B.E.K., J.D., and M.H.M. Funding Acquisition, M.H.M.; Resources, M.H.M.; Supervision, M.H.M.

Abstract

Prenatal stress (PS) can impact fetal brain structure and function and lead to higher vulnerability to neurodevelopmental and neuropsychiatric disorders. To understand how PS alters evoked and spontaneous cortical activity and intrinsic brain functional connectivity, mesoscale voltage imaging was performed in adult C57BL/6NJ mice who were exposed to an auditory stress paradigm on gestational days 12-16. PS mice demonstrated a four-fold higher basal corticosterone level, reduced amplitude of all cortical sensory-evoked responses (visual, auditory, whisker, forelimb, and hindlimb), decreased overall resting-state functional connectivity, declined network efficiency, reduced inter-module connectivity, enhanced intra-module connectivity, and altered frequency of auditory and forelimb spontaneous sensory motifs relative to control animals. In fact, for PS, the resting-state functional connectivity changes drastically towards an overall less connected structure that consists of largely disjoint but tight modules, leading to a declined network efficiency. The changes in structure also indicate that the posterior secondary motor, primary barrel, and secondary hindlimb cortices are cortical areas with higher susceptibility to dysfunction. Our findings highlight the PS modulation of brain functional connectivity that can pose offspring at risk for stress-related neuropsychiatric disorders.

Keywords: Prenatal stress, spontaneous activity, cortical evoked responses, resting-state functional connectivity, sensory motifs, voltage-sensitive dye imaging

1. Introduction

Stressful events during critical periods of development, including changes in the intrauterine environment during the prenatal period, influence the brain through affecting the nervous, neuroendocrine, and immune systems (Jafari *et al.*, 2019). Prenatal stress (PS) is characterized as a global public health concern (Kinney *et al.*, 2008; Rubin, 2016) and has been reported in 10–35% of children worldwide (Maselko *et al.*, 2015). It is well-known that PS impacts the maternal neuroendocrine system and leads to both "re-programming" of the fetal hypothalamic-pituitary-adrenal (HPA)-axis (Bock *et al.*, 2014) and changes in corticogenesis, which are associated with lifelong alterations in brain and behavior (Scheinost *et al.*, 2017). For instance, PS down-regulates placental 11β-hydroxysteroid dehydrogenase type 2 (11β-HSD2), an enzyme that metabolizes cortisol (i.e., corticosterone in nonhuman animals) (Jensen Pena *et al.*, 2012; O'Donnell *et al.*, 2012), delays GABAergic interneuron development and behavioral inhibition (Lussier and Stevens, 2016), and elevates levels of immune response genes, such as pro-inflammatory cytokines IL-6 and IL-1β (Bronson and Bale, 2014).

During the past decade, resting-state functional magnetic resonance imaging (RS-fMRI) has been extensively used to investigate brain functional networks in health and disease (Nasiriavanaki *et al.*, 2014). Resting-state functional connectivity (RSFC) is an emerging approach that identifies low-frequency, spontaneous cerebral fluctuations, and their associated functional connections with relatively high spatial and temporal resolution (Friston, 2011). In recent years, RSFC has been widely examined to study mechanisms underlying brain functional connectivity (FC), as well as the modulation of FC in murine models of psychiatric and neurological disorders (Nasiriavanaki *et al.*, 2014; Grandjean *et al.*, 2020). Among wide-field mesoscale optical imaging techniques in mice, voltage-sensitive dye (VSD) imaging maps neuronal activity dynamics with high temporal and spatial resolution and is a convenient way to image cortical spontaneous activity (Bermudez-Contreras *et al.*, 2018) and RSFC in mouse models of neurodevelopmental disorders (McGirr *et al.*, 2020).

Neurodevelopment relies on the growth and maturation of neural components into complex structural and functional networks called the connectome (Scheinost *et al.*, 2017). PS

plays a substantial role among various genetic-, health-, and environment-related factors that contribute to the development of connectome (Scheinost *et al.*, 2017; van den Bergh *et al.*, 2018). Both human and nonhuman studies using various neuroimaging techniques have shown that maternal distress during pregnancy is associated with structural and functional alterations in several brain regions, and changes in the FC of amygdalar–thalamic networks, default mode networks (DMN), and attentional networks (van den Bergh *et al.*, 2018). Few studies, however, have shown how PS modulates cortical sensory-evoked responses (SERs) and RSFC. The present study using VSD imaging in adult C57BL/6NJ mice investigates the lasting impacts of an auditory stress paradigm during gestation on SERs, intrinsic FC, and spontaneous sensory motifs during adulthood. This study was novel in several aspects to characterize how PS: 1) alters cortical SERs; 2) modulates RSFC in multiple sensory, motor, and associative brain regions; and, 3) modifies spontaneous sensory motifs in adult mice. We hypothesized that cortical SERs, intrinsic FC, and the frequency of spontaneous sensory motifs differ in the PS network relative to the control network.

2. Material and methods

2.1. Animals

Eighteen female C57BL/6NJ mice between 8-10 weeks of age were individually mated with eighteen male C57BL/6NJ mice in standard pie-shape cages. The animals were given access to food and water ad libitum and were maintained on a 12:12-h light:dark cycle in a temperature-controlled breeding room (21 °C) with less than 58±2 dBc room noise level. For the recording of gestational length, a former protocol was followed (Jafari *et al.*, 2017; Jafari *et al.*, 2018b). When the pups were born, the dams were kept individually with the litters. At the age of 21-23 days, the pups were weaned from their mothers, and only one male pup was randomly selected from each litter. All experiments and surgeries were performed during the light phase of the cycle under the approved protocols by the University of Lethbridge Animal Care Committee in accordance with the regulations of the Canadian Council of Animal Care.

2.2. Experimental design

Pregnant C57BL/6NJ mice were randomly assigned into two groups consisting of one PS group and one control group. PS animals were exposed to noise exposure on gestational days

(GDs) 12-16 because the corticogenesis process occurs within embryonic days 10-17 in mice, and layers II/III, IV, and V mainly develop during GDs 12-16 (Kolb *et al.*, 2012; Kolb *et al.*, 2013). This timeframe is also in line with the second trimester of human pregnancy, once substantial neural development occurs (Clancy *et al.*, 2007).

2.2.1. PS procedure

The PS paradigm consisted of an intermittent 3000Hz frequency sound of 90 dB for 1s duration and 15s inter-stimulus interval and lasted for 24hrs starting at 8:00am (Jafari *et al.*, 2017; Jafari *et al.*, 2018b). This tonal frequency was applied since it is audible to mice(Heffner and Heffner, 2007), and is relatively similar to environmental noises, which are largely made up of low to mid-frequency tones (Chang *et al.*, 2014). The intermittent presentation of noise stimulus, as well as 24hrs rest after every exposure also were used to prevent noise-induced hearing loss (White *et al.*, 1998). On GDs 12, 14, and 16, pregnant mice (n=9) in groups of two to three in their standard cage were moved to a sound chamber specified for the PS group. A speaker, which emitted the noise stimulus was placed inside the cage. The sound pressure level was monitored daily inside the cage without an animal (Tektronix RM3000, Digital Phosphor Oscilloscope). A similar procedure was applied for the control pregnant mice (n=9). A silent speaker, however, was placed inside the cage, and no noise exposure was given.

2.2.2. Plasma corticosterone assay

A day before each animal surgery, blood was collected from the submandibular vein at 7:30 to 8:30am. Approximately 0.1ml of blood was taken in heparin-coated tubes. The tubes were centrifuged at 6000rpm at 4°C for 15min to gather the plasma. Collected plasma samples were stored at −80°C and then analyzed as previously reported (Jafari *et al.*, 2018a; Jafari *et al.*, 2018b).

2.2.3. Surgery

An acute craniotomy was performed for the PS (n=6) and control (n=9) offspring at age 2-3 months. Mice were given an acute 7×6 mm unilateral craniotomy (bregma +2.5 to -4.5 mm, lateral to the midline 0 to 6mm for VSD imaging experiments as previously described (Kyweriga *et al.*, 2017)). Isoflurane (1.0–1.5%) was used to anesthetize mice both for induction and during surgery. A lower concentration of isoflurane (0.5-0.7%), however, was applied throughout data

collection. Mice were head-fixed during imaging, in which the skull being fastened to a steel plate while they were posed on a metal plate onto the stage of the upright microscope (Mohajerani *et al.*, 2010). A heating pad was used to preserve the body temperature at 37°C.

2.2.4. VSD imaging

Wide-field optical imaging of summated cortical voltage activity was used to capture the mesoscale dynamics of the cortex. For in vivo VSD imaging, the dura was carefully removed within the craniotomy window. The dye RH-1691 (Optical Imaging, New York, NY, USA) (Shoham *et al.*, 1999) was dissolved in HEPES-buffered saline (0.5 mg/ml) and applied to the exposed cortex for 30-40min(Mohajerani *et al.*, 2010). The unabsorbed VSD was washed and imaging begun almost 30min later. As respiration could lead to moving artifacts, the brain was covered with 1.5% agarose made in HEPES-buffered saline and sealed with a glass coverslip to minimize that effect. A charge-coupled device (CCD) camera (1M60 Pantera, Dalsa, Waterloo, ON, Canada) and an EPIX E8 frame grabber with XCAP 3.8 imaging software (EPIX, Inc., Buffalo Grove, IL, USA) were used to capture 12-bit images with 6.67ms temporal resolution. Collected images were taken through a microscope composed of front-to-front video lenses (8.6 × 8.6mm field of view, 67μm per pixel). VSD was excited using a red LED (627nm center, Luxeon Star LEDs Quadica Developments Inc., AB, Canada) and excitation filter (630±15nm, Semrock, NY, USA). VSD fluorescence was filtered using a 673 to 703nm band-pass optical filter (Semrock, NY, USA). The imaging was focused on the cortex to a depth of ∼1mm to avoid distortion of the signal given the movement of superficial blood vessels.

2.2.5. Sensory stimulation

The map of the sensory cortical areas was taken by virtue of forelimb, hindlimb, whisker, visual, and auditory stimuli. A thin needle (0.14mm) was inserted in the paws for hindlimb and forelimb stimulation, which delivered a current of 0.2-1mA for 1ms. For whisker stimulation, a single whisker was attached to a piezoelectric device (Q220-A4-203YB, Piezo Systems, Inc., Woburn, MA, USA) and stimulated by a 1ms square pulse. Visual stimulation was provided through a 1ms pulse of combined green and blue light. For auditory stimulation, a 12kHz pure-tone at 80dB was presented using a Tucker-Davis Technologies (TDT) RX6, once the animal was sitting in a sound-proof booth. The speaker (TDT, ES1 electrostatic loudspeaker) was calibrated to emit uniformly distributed sound stimulus. Sensory stimulations were separated by

an interval of 10s. Stimulated trials lasted for 1s, and the stimuli were presented after passing one-third of the time of that trial.

2.2.6. Spontaneous recording

Spontaneous activity was imaged in the absence of any stimuli with 6.7ms temporal resolution (150Hz).

2.3. Data analysis

2.3.1. VSD processing

Six to twenty stimulation trials were averaged to decrease the effect of spontaneous change of brain states. These trials were used for the normalization of the stimulated data. Using MATLAB® (Mathworks, Natick, MA, USA), VSD responses were calculated as a percentage change relative to baseline ($\Delta F/F_0 \times 100\%$). The baseline was estimated for both no-stimulation trials and spontaneous activity, using the "locdetrend" function from the Chronux toolbox (Bokil *et al.*, 2010). Temporal low-pass filters with cutoff frequencies of 30Hz and 6Hz were respectively used for evoked and spontaneous recordings. To get a smoother signal, a spatial Gaussian filter with sigma equal to 1µm also was applied to both evoked and spontaneous recordings.

2.3.2. ROI identification

The neocortex was divided into 19 regions including: primary sensory and motor areas (motor barrel cortex (mBC), motor forelimb (mFL), motor hindlimb (mHL), primary hindlimb (HLS1), primary forelimb (FLS1), primary lip (LpS1), primary barrel cortex (BCS1), primary visual (V1), primary auditory (A1)), supplementary areas (secondary barrel (BCS2), secondary hindlimb (HLS2A and HLS2B), secondary forelimb (FLS2), lateral secondary visual (V2L), medial secondary visual (V2M), anterior segment of the secondary motor (aM2), posterior segment of the secondary motor (pM2)), and association areas (parietal association (ptA) and retrosplenial cortex (RSC)). To specify cortical regions, sensory stimulation was used to set coordinates for the primary and secondary somatosensory areas (HLS1, HLS2A, HLS2B, FLS1, FLS2, BCS1, BCS2, V1, and A1). The coordinates of other areas were set relative to these sensory areas' coordination, using stereotaxic atlas as previously described (Paxinos, 2001). We defined these regions of interest (ROI) as a 5×5-pixel area around the specified coordinates and

the time series associated with each ROI was the average of $\Delta F/F_0$ across all pixels within the ROI.

2.3.3. Evoked activity

Evoked responses were characterized by peak amplitude, the area under the peak, and time to peak (rise time). The peak of the evoked responses was set as the maximum value from the onset of the stimulus to 200ms thereafter, as long as the value was at least two standard deviations above the baseline. The area under the peak also was defined from the onset of the stimulus to 200ms afterward. Finally, rise time was determined by subtracting the response onset time from the peak time. For all quantifications, the baseline was defined as the mean of the evoked signal from 300ms to 10ms before the stimulus.

2.3.4. Correlation and network analysis

Correlation matrices were created based on the zero-lag correlation between spontaneous VSD $\Delta F/F_0$ signals of every couple of 19 cortical ROIs. For network analysis, both full and partial correlations were employed to respectively characterize the global and local structure of the networks. The brain connectivity toolbox (Rubinov and Sporns, 2010) was used to calculate network measures including global efficiency, characteristic path, clustering coefficient, eccentricity, nodes betweenness centrality, modularity, and participation coefficient (see Supplementary methods for more details).

2.3.5. Spontaneous sensory motifs

Sensory motifs are patterns in the spontaneous activity that resemble evoked responses to sensory stimuli. A template matching technique was used to identify these motifs as previously described (Mohajerani *et al.*, 2013). For each sensory modality, the template was identified using the first three frames after the onset of evoked activity and the Pearson correlation coefficient was found between templates and the spontaneous activity. Then, frames of the spontaneous activity with a greater correlation coefficient than a given threshold were considered as a ‘match’ (i.e., sensory motif). The temporal order of sensory motifs within spontaneous activity was also identified. Given the existence of five sensory templates, there were 20 double, 60 triple, 120 quadruple, and 120 quintuple non-repetitive combinations of motifs to be explored in the spontaneous activity (see Supplementary methods for more details).

2.3.6. Statistical tests

As data were often non-normally distributed, a two-sided Wilcoxon rank-sum test, equivalent to a Mann-Whitney U-test, was applied for cross-sectional analysis. Both full and partial correlation analyses were performed based on the linear dependence of variables using the Pearson correlation coefficient. P-values for correlational analysis were computed using a Student's t distribution for a transformation of the correlation. This was exact for normal data but was a large-sample approximation otherwise. All statistical analyses were performed using MATLAB at a significance level of 0.05 or lower. Error bars and ± ranges represent the standard error of the mean (SEM). Asterisks indicate $*p < 0.05$, $**p < 0.01$, $***p < 0.001$.

3. Results

3.1. Elevated corticosterone levels

The timeline of the experiment is shown in Fig. 1A. The basal corticosterone level was more than four-fold higher in the PS group compared with the control group ($p \leq 0.001$, Fig. 1B).

3.2. Reduced sensory-evoked amplitudes

In the control group, all modes of sensory stimulation (hindlimb, forelimb, whiskers, visual, or auditory systems) resulted in consensus patterns of cortical depolarization (Fig. 1C and 1D) consistent with previous findings (Mohajerani *et al.*, 2013). We found that sensory stimulation led to the activation of primary sensory areas as well as "islands" of response within functionally related areas such as primary motor regions (mFL, mHL, mBC), secondary sensory areas (FLS2, HLS2, BCS2, V2) or cortical areas along the mid-line (RSC, cingulate, and secondary motor) (Fig. 1D). For all sensory modalities, the activity appeared initially in the primary cortices and then spread to secondary somatosensory cortices. The montage of VSD images in Fig. 1D demonstrates a reduction of cortical activation and localization of response to all stimuli in the PS group relative to the control mice.

Fig. 1E illustrates the evoked response of primary cortical regions to each corresponding stimulus. The PS mice showed a declined VSD response (i.e., $\Delta F/F_0$) in all cortical regions compared to the control group. To statistically verify this group difference, the peak amplitudes (V1: rank-sum=92.5, p=0.012; A1: rank-sum=95, p=0.004; BCS1: rank-sum=99, $p \leq 0.0001$;

FLS1: rank-sum=94, p=0.007; HLS1: rank-sum=95, p=0.004) and the area under the peak (V1: rank-sum=93.5, p=0.008; A1: rank-sum=97, p=0.001; BCS1: rank-sum=99, p≤0.001; FLS1: rank-sum=95, p=0.004; HLS1: rank-sum=98, p≤0.001) were compared between the two groups. To quantify evoked responses within wider cortical regions, the VSD responses were compared at 19 cortical ROIs corresponding to Fig. 1C (see Methods). The statistically quantified responses of all other cortical regions in terms of peak amplitude, area under the peak, and rise time of the response were shown in the supplementary information (Supplementary Fig. 1, 2, and 3; and Supplementary Tables 1, 2, and 3).

3.3. Group difference comparisons using intracortical functional connectivity matrices

Mice in both control and PS groups exhibited dynamic, spatially complex patterns of spontaneous cortical activity. To quantify the effect of PS on intracortical functional connectivity, a zero-lag full correlation analysis was used (Fig. 2A). Correlation matrices in Fig. 2A show the average of animals per group. Whereas most of the regions were highly correlated, the overall correlation strength was reduced in the PS compared to the control group ($MeanCorr_{Control}$= 0.8±0.02 vs. $MeanCorr_{PS}$= 0.65±0.04, P< 0.005). Fig. 2B (Supplementary Table 4) illustrates the average correlation between each ROI and all other regions, indicating the regional nonspecific reduction of functional connectivity in the PS group. Fig. 2C represents the subtraction of the correlation matrices of the two groups displayed in Fig. 2A, which shows that 75% (118 out of 156) of correlation comparisons are significantly different.

3.4. Reduced efficiency and enhanced modularity in the PS network

A comparison of connectivity matrices in Fig. 2C shows a PS-induced overall decrease of correlation coefficient values within most of the regions compared with the control group. For a better understanding of intracortical relationships in the two groups, a network diagram using the correlation matrices was derived. In Fig. 3A, network diagrams are plotted based on the average correlation in each group. The thickness of the connecting lines is proportional to the strength of the connection, and the nodes (regions) are positioned based on the average brain coordinates for animals in a group. Although the number of links was the same, they were thicker (i.e., larger correlation coefficients) in the control network. Since edge width distributions were different as

shown in Fig. 3B, no threshold was introduced to the correlation coefficients to avoid biased results (Buchanan *et al.*, 2020) (see Supplementary methods).

To find out how information flow might be affected by PS, we made a comparison of some basic global network measures indicating network efficiency such as “clustering coefficient”, “characteristic path length”, “global efficiency”, and “eccentricity”. The “clustering coefficient”, which measures to what extent the node’s neighbors are neighbors of each other, and the “characteristic path”, which is the average shortest path length between all pairs of nodes in the network”, are extensively used in brain network studies (Bullmore and Sporns, 2009). It has been shown that brain networks are highly clustered with a short characteristic path, which is a measure of “small-world property” (Hilgetag *et al.*, 2000; Sporns and Zwi, 2004). Fig. 3C demonstrates a larger clustering coefficient (Fig. 3Ci) and a shorter characteristic path (Fig. 3Cii) of the control compared with the PS network, which refers to a compromised small-world property in the PS mice. The “global efficiency” of a network also can be directly computed as the average of inverse shortest path length, which was significantly reduced in the PS (Fig. 3Ciii). Similarly, “eccentricity”, which exhibits the maximal path length between a node and any other node in the network, was increased in the PS relative to the control group (Fig. 3Civ).

Centrality measures are used to obtain the functional importance of a region. For instance, “betweenness centrality” measures the fraction of all shortest paths in the network that contains a given node. Whereas the average betweenness of nodes was increased in the PS compared to the control network (Fig. 3Cv), none of the ROIs consistently emerged as a central region among most animals in either of the groups.

Since the use of a full correlation analysis leads to a highly connected network, segregated structure, and the existence of hubs, two major hallmarks of brain networks, (Bullmore and Sporns, 2009) were not observed. Thus, partial correlation was employed to create a sparser network by capturing the direct functional connection between regions (Martin *et al.*, 2017; Oliver *et al.*, 2019) (see Supplementary Fig. 4 for partial correlation matrices). Weighted networks in Fig. 4A display functional connectivity based on partial correlation. The edge widths imply the strength of the connection between regions and nodes with the same color belong to the same community.

A higher number of non-overlapping groups of nodes in a given network is an indication of optimal network structures (Newman, 2006) and modularity is a quantified measure that shows to what extent a network is divided into such specified communities[24]. Using community detection algorithms (see Supplementary methods), a consensus partition for networks of both groups was created (Fig. 4A). Whereas the number of communities remained the same in both networks, the host modules of some nodes were different between the two groups. To make a quantified comparison of modularity, the average quality functions (Q), obtained from the community detection algorithm, were compared (Fig. 4B). Higher modularity in the PS network (Fig. 4Bi) implied that intermodular communication was more clearly separated from intramodular connections than the control network.

To quantify the amount of communication between regions, the established measure of participation coefficient was applied (Power *et al.*, 2013), which shows the degree a node is restricted to its community. The average participation coefficient was significantly reduced in the PS network (Fig. 4Bii), which reflects its stronger intra-community communication compared with the control network. Another important feature of complex networks is the existence of hubs. Generally, hubs are characterized as high degree nodes with edges that pose them in central positions for promoting communication through a network. Based on the participation coefficient, hubs are categorized into two types of "provincial" (low participation coefficient) and "connector" (high participation coefficient)[50] (see Supplementary methods). Although no hub was identified in the group level of control network, two provincial hubs (pM2 and HLS2A) and one connector hub (BCS1) were identified in the network of PS group (Fig. 4Aii). Overall, compared with the control network, whereas the average number of provincial hubs was significantly greater in the PS network (Fig. 4Biv), the average number of connector hubs was decreased (Fig. 4Bii). None of the regions, however, consistently emerged as a connector hub in the majority of control mice.

3.5. Rate and temporal order of motifs

To examine how PS alters patterns of activity in the brain, the rate and succession of the spontaneous sensory motifs were compared between the two groups. These spontaneously occurring motifs were determined using a template matching method through the templates extracted from multimodal sensory-evoked responses, Fig. 5A (see Methods, Supplementary

methods, and Supplementary Fig. 5). Using this approach, the spontaneous motifs originated from the forelimb, hindlimb, barrel, visual and auditory cortices were identified (Fig. 5Aii). The heat map in Fig. 5B demonstrates the concurrent correlation of different templates of sensory-evoked responses with a 30s period of spontaneous activity. Correlation of instantaneous patterns of spontaneous activity with multiple templates of sensory-evoked responses for the first 6s of the data in panel B, has been plotted in Fig. 5C. Peaks in this plot reflect parts of spontaneous activity closely resembling the sensory-evoked templates. Shaded rectangles in Fig. 5C are recognized as motifs, whose VSD montage plots are shown in Fig. 5Aii (see Supplementary methods for more details). The overall occurrence rate (i.e., number of motifs per second) was 0.31±0.01 and 0.29±0.01 in the control and PS groups respectively ($p > 0.1$). Despite an identical overall rate of motifs' occurrence in both groups, the frequency of occurrence was increased for auditory motifs and decreased for forelimb motifs, with no changes for the visual, hindlimb, and whisker motifs (Fig. 5D).

While spontaneous cortical activity has been shown to constitute a complex combination of multiple sensory motifs (Afrashteh *et al.*; Mohajerani *et al.*, 2013), their sequential order remains unknown. So, we tested whether PS alters the temporal order of motif combinations by comparing all possible nonrepetitive permutations, including, 20 double, 60 triple, 120 quadruple, and 120 quintuple sequences (see Methods and Supplementary methods). The results of quintuple sequences, however, were not included given their rare occurrence. Beside comparing PS and control groups, we compared the temporal order of motif sequences in each group with random data (see Supplementary methods).

Fig. 6A exhibits the average number of sequences that revealed a significant difference between experimental and random data in both groups (Fig. 6A) (quadruple sequences: control, 0.088±0.015, control-shuffled, 0.140±0.006, $p > 0.02$; PS, 0.087±0.01, PS-shuffled, 0.13±0.006, $p > 0.008$; triple sequences: control, 0.51±0.064, control-shuffled, 0.72±0.027, $p > 0.02$; PS, 0.61±0.1, PS-shuffled, 0.67±0.028, $p > 0.015$; double sequences: control, 3.05±0.22, control-shuffled, 3.7±0.12, $p > 0.04$; PS, 2.92±0.18, PS-shuffled, 3.45±0.13, $p > 0.04$). Despite significant changes in the average rate of sequences, few individual sequences in each group emerged significantly different from the random occurrence. Fig. 6B, Supplementary Fig. 6A, and Supplementary Fig. 6C demonstrate this result for the triple, quadruple and double permutations,

respectively. In fact, only 7% and 8% of quadruple combinations, 22% and 35% of triple combinations, and zero percent of double combinations occurred below chance in the PS and control groups, respectively. The number of cells in each block is equal to the number of permutations and the letters in each cell are a short form of sequences' names. The colors reflect whether the sequence occurrence rate has decreased or increased from the chance level. According to Fig. 6A, PS also had no effect on the average rate of multiple combinations' occurrence (quadruple sequences: control, 0.088±0.015, PS, 0.087±0.01, $p > 0.85$; triple sequences: control, 0.51±0.064, PS, 0.5±0.045, $p > 0.66$; double sequences: control, 3.05±0.22, PS, 2.92±0.18, $p > 0.75$). Bar graphs in Fig. 6C and Supplementary Fig. 6B show only the rate of occurrence for 5 out of 60 triple combinations (8%) and 6 out of 120 quadruple combinations (5%) that were significantly different between the two groups.

4. Discussion

To examine how exposure to stress during the prenatal period alters cortical evoked responses to sensory stimuli, RSFC, and spontaneous sensory motifs, the VSD data of mice subjected to PS were compared with the control animals at 2-3 months of age. Briefly, the PS was associated with: 1) a reduced amplitude of evoked responses to sensory stimuli, 2) overall decline of RSFC and network efficiency, 3) decreased between-network connectivity, 4) increased within-network connectivity, 5) the appearance of two provincial hubs (pM2 and HLS2A regions) and one connector hub (BCS1 region), and 6) the altered occurrence frequency of auditory and forelimb motifs.

4.1. Decreased cortical evoked responses to sensory stimuli

In this study, the amplitude of evoked responses to different stimuli were significantly reduced for the PS mice relative to the control group. Few human and non-human animal studies have shown how PS modulates SERs during adulthood. Experimental studies, however, imply that the administration of glucocorticoids during the first two postnatal weeks in rats is associated with delayed development of the startle reflex (Pavlovska-Teglia *et al.*, 1995) and cortical evoked responses to auditory, visual, and sciatic nerve stimulation (Salas and Schapiro, 1970). Administration of chronic corticosterone in adult C57BL/6NJ mice also demonstrated that the modulation of the amplitude of auditory evoked responses (AERs) is dose-dependent, and the

serum corticosterone concentration is negatively correlated with the amplitude of AERs (Maxwell *et al.*, 2006). The amplitude of forelimb stimulation also was reduced in a study on adult C57BL/6NJ mice under chronic restraint stress (Han *et al.*, 2019).

In rodents, the HPA-axis shows a distinct developmental profile around birth, which is characterized by very low basal levels of corticosterone and a relative non-responsiveness to mild external stresses (Levine, 2001). This feature protects the developing brain from adverse impacts of high levels of stress hormones (Bock *et al.*, 2014). In our study, the PS mice showed a four-fold higher basal corticosterone level than the control group in adulthood. Corticosterone is the primary component of the stress system that along with the sympathetic nervous system contributes to mobilizing energy stores in response to stressful events (Charil *et al.*, 2010; Handa and Weiser, 2014). Current experimental research supports the idea that the dysregulation of the HPA-axis during sensitive fetal periods is associated with lasting alterations in brain and behavior throughout the lifespan (Huizink *et al.*, 2004; Charil *et al.*, 2010; Weinstock, 2017). Past studies have shown that prenatal noise stress alone or in combination with other stresses is linked to higher levels of corticosterone at rest, delay in sensory and motor development, and life-long impairments in behavioral and cognitive performance (Jafari *et al.*, 2019). Although our finding is consistent with past studies showing the effect of HPA dysregulation on SERs, the neurophysiological mechanisms underlying the PS-induced higher basal corticosterone levels during adulthood and its impact on sensory processing require further investigations.

4.2. Reduced efficiency and increased modularity of the network

In our study, the overall functional connectivity (i.e., correlation strength), regional cortical connectivity (i.e., the average correlation between one brain ROI and all other regions), and network efficiency were reduced in the PS mice relative to the control ones. Based on graph theory analysis, a convenient tool to illustrate the topological organization of the connectivity, several network measures (clustering coefficient, characteristic path length, global efficiency, eccentricity, and betweenness) supported reduced efficiency of information flow in PS.

Human evidence of brain imaging techniques refers to long-lasting PS-associated structural and functional changes in several brain regions (e.g., the prefrontal cortex, parietal and temporal lobes, and the cerebellum, hippocampus, and amygdala) (van den Bergh *et al.*, 2018). Alterations in brain FC have been shown in amygdalar–thalamic networks and intrinsic brain

networks (e.g., DMNs and attentional networks) (Favaro *et al.*, 2015; Graham *et al.*, 2016; Scheinost *et al.*, 2016; Turesky *et al.*, 2019). Animal studies also indicate that PS or early exposure to environmental stresses alter synaptogenesis in the neocortex and the hippocampus (Bale *et al.*, 2010; Mychasiuk *et al.*, 2012), impact brain development (Mychasiuk *et al.*, 2012; Kolb *et al.*, 2013; Weinstock, 2017), and produce alterations in the connectome (Scheinost *et al.*, 2017).

It has been characterized that the PS-induced dysregulation of the HPA-axis drives epigenetic changes in the developing brain (Scheinost *et al.*, 2017). Cortisol (i.e., corticosterone in nonhuman animals), the end product of the HPA-axis, has a prominent contribution to brain homeostasis and response to various types of psychological and environmental stresses. Increased maternal cortisol levels during pregnancy can influence the fetal brain through the placenta or stimulating fetal cortisol production (Sapolsky *et al.*, 2000). The placental enzyme 11β-HSD2, which is a partial barrier to the passage of active cortisol, is downregulated in adverse prenatal conditions (Reynolds, 2013).

Both human and nonhuman studies point to altered maternal immune activity in PS, which poses offspring at risk for cognitive and behavioral disorders (Estes and McAllister, 2016; Scheinost *et al.*, 2017). In a human study in neonates at 40–44 weeks postmenstrual age, maternal third trimester interleukin-6 (IL-6) and C-reactive protein (CPR) levels, which regulate immune responses, were associated with brain FC in default mode, salience, and frontoparietal networks, as well as with both fetal and toddler behavior (Spann *et al.*, 2018). IL-6, which crosses both the placenta and blood-brain barrier (Zaretsky *et al.*, 2004), is part of both the pro-inflammatory and anti-inflammatory pathways that their imbalance contributes to cognitive and behavioral development (Meyer *et al.*, 2008). It also has been found that early life experiences and the resulting behavioral consequences can be transmitted to the next generation through the epigenetic process, which indicates a transgenerational cycle of changes in the brain and behavior (Bock *et al.*, 2014). Epigenetics, which refers to a set of sustained, post-translational modifications of DNA and nuclear proteins (Levenson and Sweatt, 2005), is characterized as an interface between early environmental experiences and the occurrence of genetically programmed developmental processes throughout the lifespan (Bock *et al.*, 2014). Taken together, several mechanisms, including alterations in the neuroendocrine system, the immune

system, and the epigenetic processes, may implicate in reduced efficiency and undermined small-world property (Rubinov and Sporns, 2010) in PS mice, which suggest directions for further studies.

To further examine the impact of PS on brain network connectivity, we measured "modularity" (Newman and Girvan, 2004), the degree a network can be classified into non-overlapping but internally interactive subsets of regions (Thomason *et al.*, 2014), and "participation coefficient" (Power *et al.*, 2013), which reflects the degree a node is relying on its community. In both measures, the PS network demonstrated more disjoint but tight modules relative to the control network. We also identified two "provincial hubs" (pM2 and HLS2A regions) and one "connector hub" (BCS1 region) in the PS network, whereas no hub was obtained in the control network.

In brain networks, hubs are characterized as nodes with a special role in promoting communication through a network. Whereas provincial hubs contain lower participation coefficients and confine to their community, connector hubs have higher participation coefficients and contribute widely among communities (Sporns *et al.*, 2007). Few studies have shown how network modularity and nodes' connections are changing in rodent brains in the context of PS. But it has been found that hubs are biologically costly, because they have higher metabolic demands and longer-distance connections compared to other brain regions (Crossley *et al.*, 2014). Studies also suggest that the integrative role of hub nodes makes them more vulnerable to dysfunction in brain disorders (van den Bergh *et al.*, 2018), in which deviant hubs may show more tendency to function in brain pathological states (Crossley *et al.*, 2014; Sporns, 2014; Liska *et al.*, 2015). Thus, our findings might be interpreted as showing that PS is associated with enhanced within network connectivity in HLS2A and pM2 regions, and increased contribution of primary barrel cortex (BCS1) in communication between networks and response to environmental stimuli. Given that no hub was consistently identified among the control mice, it might be inferred that increased modularity in the PS network is an indication of more segregated functional sub-networks that were not ameliorated with increasing age.

4.3. Altered frequency of spontaneous sensory motifs

Multiple anatomically consistent RS networks in the brain (e.g., DMN, sensorimotor, and cortical sensory areas) produce temporally coherent spontaneous fluctuations in rest or the

absence of any external stimulation (Kong *et al.*, 2014). A group of these intrinsic responses, which originate from primary sensory cortices, expand identical to SERs called sensory motifs (Kenet *et al.*, 2003). It has been shown that the brain does computations using sensory motifs (Turkheimer *et al.*, 2015). Among five spontaneous sensory motifs (visual, auditory, whisker, forelimb, and hindlimb) examined in this study, the PS was associated with an increase in the frequency of auditory motifs and a decrease in the rate of forelimb motifs. Using a postnatal maternal deprivation stress paradigm over whisker, forelimb, and hindlimb sensory motifs, an increased occurrence of whisker and forelimb motifs was reported in (McGirr *et al.*, 2020). These findings imply that stress does not uniformly alter the frequency of different sensory motifs, which may arise from the stress procedure applied (e.g., age, duration, and type of stress exposure). Neurophysiological evidence also refers to the role of spontaneous sensory motifs in modulating cortical responses to sensory inputs (Ferezou and Deneux, 2017), as well as higher-level cognitive operations and behavior (Turkheimer *et al.*, 2015). Given these findings, the stress-related alterations of sensory motifs and their contribution to sensory processing and psychiatric disorders are suggested to be further examined in the future.

5. Conclusions

Early environmental threats, starting in utero, have shown to pose the living creature to lifelong major risks for physical and psychological health. This study aimed to investigate how PS alters SERs, RSFC in cortical sensory regions, and the occurrence of sensory motifs in the adult mouse brain. The PS was associated with reduced amplitude of all cortical SERs, overall RSFC, between-network connectivity, network efficiency, enhanced within-network connectivity (increased modularity or segregated functional sub-networks), and altered occurrence frequency of auditory and forelimb motifs. Three hubs, including two provincial and one connector hub were also found in the PS network that may function as brain regions with higher vulnerability to dysfunction. Future studies are suggested to investigate: 1) the association of altered cortical SERs, intrinsic FC, spontaneous sensory motifs, and identified hubs with PS-related behavioral disorders; and, 2) the impact of postnatal pharmacological or behavioral treatments in reversing or alleviating the PS impacts. The present study was performed under the isoflurane-anesthetized state in male mice. The replication of our experiments in both sexes during awake and

anesthetized states will help to understand how SERs, RSFC, and spontaneous sensory motifs are influenced by brain states and sex.

Legends for figures

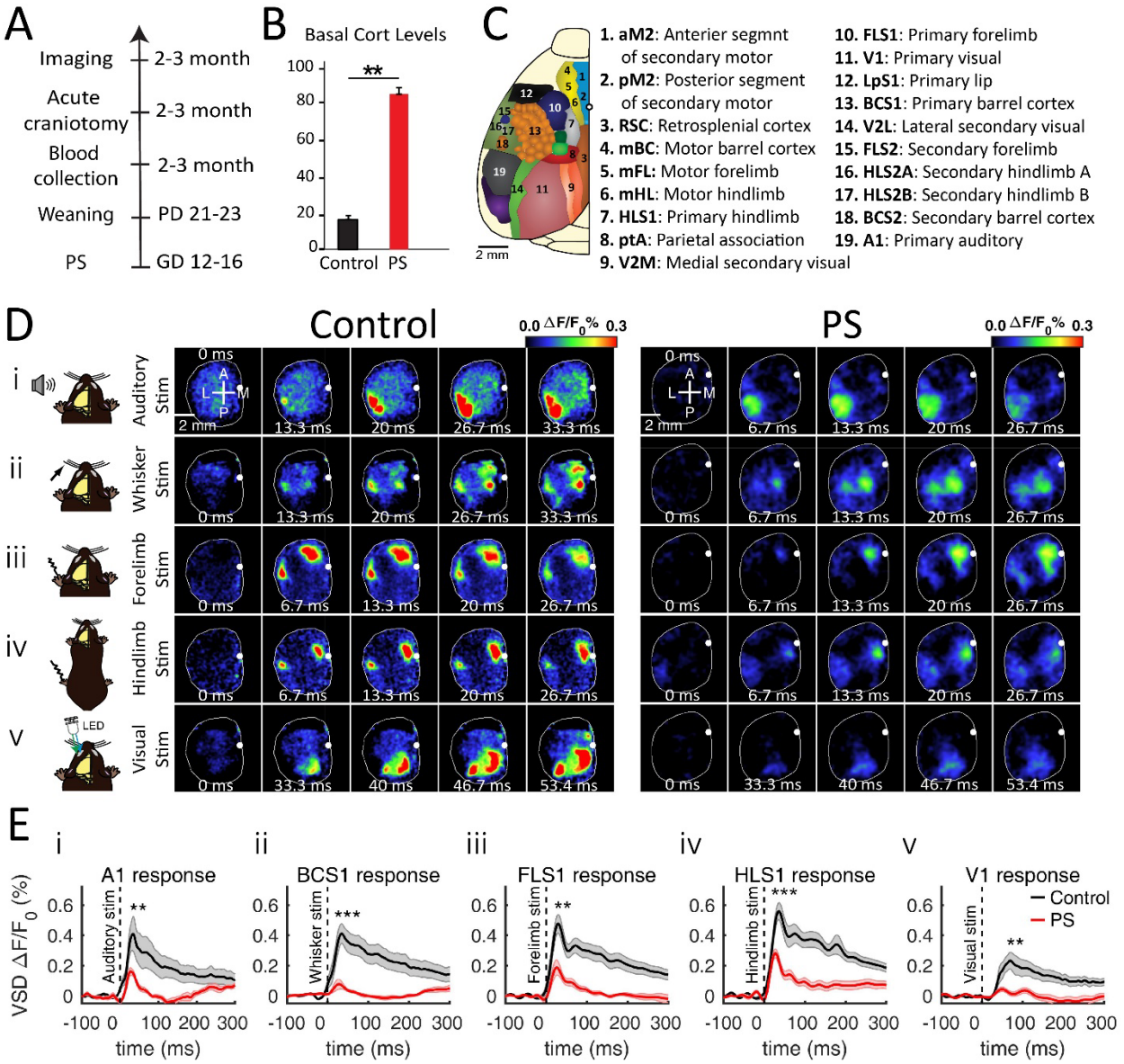

Figure 1, Rezaei et al. 2020

Fig 1. *The decline of* evoked *responses to sensory stimuli in PS mice*. **A**) Timeline of the experiment. Pregnant mice were exposed to noise stress on GDs 12-16. Their pups were weaned at the age of 21-23 days. Blood collected from pups at age 2-3 months. A day after, an acute craniotomy was performed for both groups. The VSD imaging was conducted a week thereafter. **B**) The basal corticosterone level of PS mice was significantly increased compared to the control mice. **C**) Unilateral craniotomy represents imaged cortical regions. **D**) Photomicrograph of the wide unilateral craniotomy with bregma marked with a white dot in each image. Patterns of cortical activation are shown in a mouse anesthetized with isoflurane (0.5%) after (i) auditory, (ii) whisker, (iii) forelimb, (iv) hindlimb, and (v) visual stimulations with a light-emitting diode (LED) for a control and a PS mouse. These VSD imaging montages show the frame of the stimulus (0 ms) followed by four other frames starting from the onset of the evoked response. The first image from the left in the first row indicates the anterior (A), posterior (P), medial (M)

and lateral (L) directions. **E**) Evoked VSD responses to five sensory stimuli. The shaded region in all diagrams shows SEM. The asterisks point to a significant difference in the area under the peak. (i) Response of the A1 region after the auditory stimulus (rank-sum=97, p=0.002); (ii) response of the HLS1 region after the hindlimb stimulus (rank-sum=98, $p=8\times10^{-4}$); (iii) response of the FLS1 region after the forelimb stimulus (rank-sum=95, p=0.005); (iv) response of the BCS1 region after the whisker stimulus (rank-sum=99, $p=4\times10^{-4}$); and (v) response of the V1 region after the visual stimulus (rank-sum=93.5, p=0.008). The number of mice: n=9 control, n=6 PS. Asterisks indicate *p<0.05, **p<0.01, or ***p<0.001. Cort, corticosterone; GD, gestational day; PD, postnatal day; Stim, stimulus; SEM, standard error of mean; PS, prenatal stress; VSD, voltage-sensitive dye.

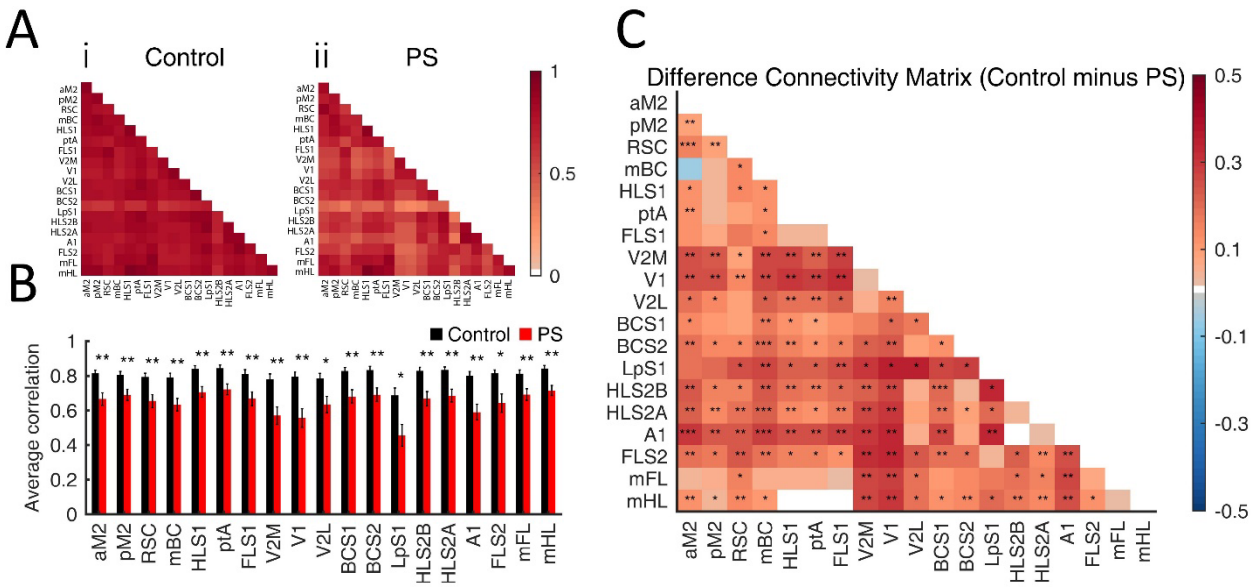

Fig 2. *Reduced cortical functional connectivity by PS*. **A**) Zero-lag full-correlation matrices for (i) the control and (ii) PS groups. **B**) A significant difference was found between the two groups on the average correlation of each ROI and all other regions. Error bars indicate SEM. Table S1 includes detailed statistics. **C**) Subtraction of inter-regional correlation coefficients. The colors specify the degree of change in correlations. Correlation between most ROIs was reduced in PS. The number of mice: n=9 control, n=6 PS. Asterisks indicate *p<0.05, **p<0.01, or ***p<0.001. A1, primary auditory; aM2, anterior segment of the secondary motor; BCS1, primary barrel cortex; BCS2, secondary barrel cortex; FSL1, primary forelimb; FSL2, secondary forelimb; HLS1, primary hindlimb; HLS2A and HLS2B, secondary hindlimb; LpS1, primary lip; mBC, motor barrel cortex; mFL, motor forelimb; mHL, motor hindlimb; pM2, the posterior segment of the secondary motor; PS, prenatal stress; ptA parietal association; ROI, region of interest, RSC, retrosplenial cortex; SEM, standard error of mean; V1, primary visual; V2L, lateral secondary visual; V2M, medial secondary visual.

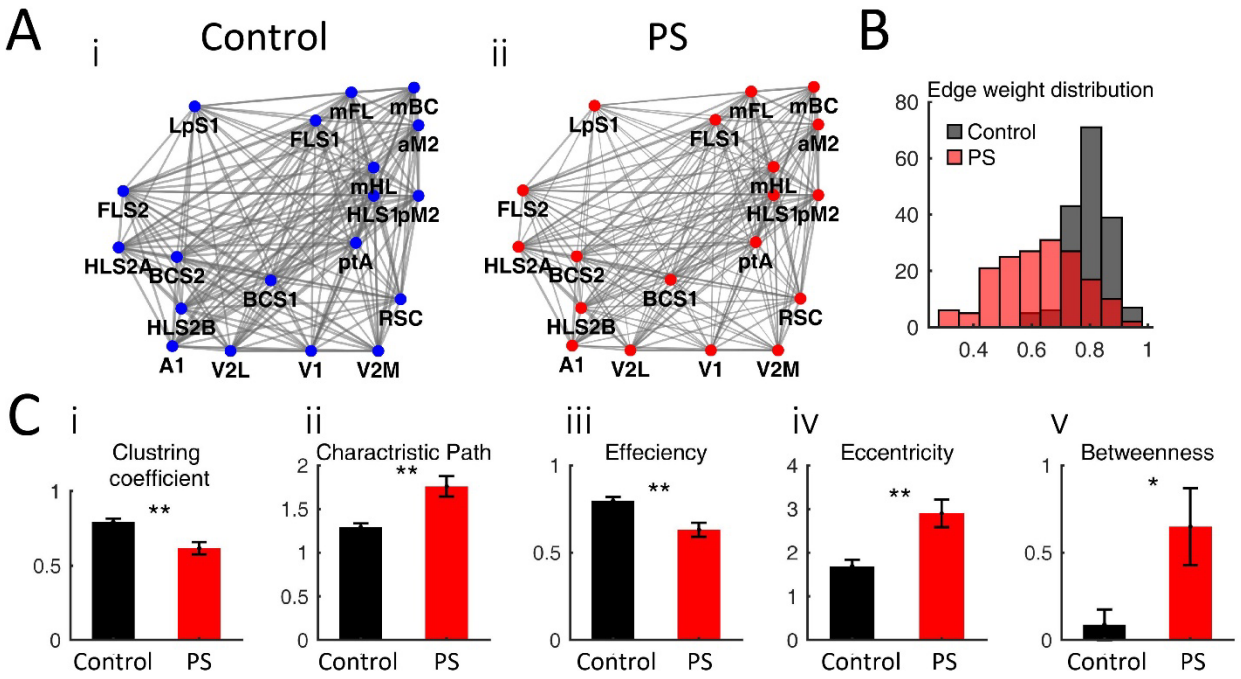

Fig 3. *Declined efficient information transmission in the cortical network in PS.* **A**) Schematic of the cortical networks based on the average correlation for (i) the control and (ii) PS groups. Nodes indicate cortical regions in the left hemisphere and edges' weight represent the strength of the connection. Edges are thicker in the control network compared to the PS network, showing the existence of stronger connections among regions. **B**) The weight distribution of edges shows a significant difference between the two groups (Z=0.65 and $p=1.2\times10^{-30}$, two-sample Kolmogorov-Smirnov test). While edge-weights in the PS network spanned all values in 0 to 1 interval with a peak around 0.62, they only varied from 0.6 to 1 with a mean around 0.8 in the control group. **C**) Comparison of some global network measures. (i) The PS network showed a smaller clustering coefficient (rank-sum=143, p=0.005), (ii) an increased characteristic path (rank-sum=86, p=0.007), (iii) a lower global efficiency (rank-sum=143, p=0.004), (iv) an increased eccentricity (rank-sum=87, p=0.009) compared with the control network. (v) The average betweenness of nodes was enhanced in the PS versus the control network (rank-sum=93.5, p=0.035). The bar graphs show the average value of the measures over all animals in a group, and error bars indicate SEM. The number of mice: n=9 control, n=6 PS. Asterisks indicate *p<0.05, **p<0.01, or ***p<0.001. A1, primary auditory; aM2, anterior segment of the secondary motor; BCS1, primary barrel cortex; BCS2, secondary barrel cortex; FSL1, primary forelimb; FSL2, secondary forelimb; HLS1, primary hindlimb; HLS2A and HLS2B, secondary hindlimb; LpS1, primary lip; mBC, motor barrel cortex; mFL, motor forelimb; mHL, motor hindlimb; pM2, the posterior segment of the secondary motor; PS, prenatal stress; ptA parietal association; RSC, retrosplenial cortex; SEM, standard error of mean; V1, primary visual; V2L, lateral secondary visual; V2M, medial secondary visual.

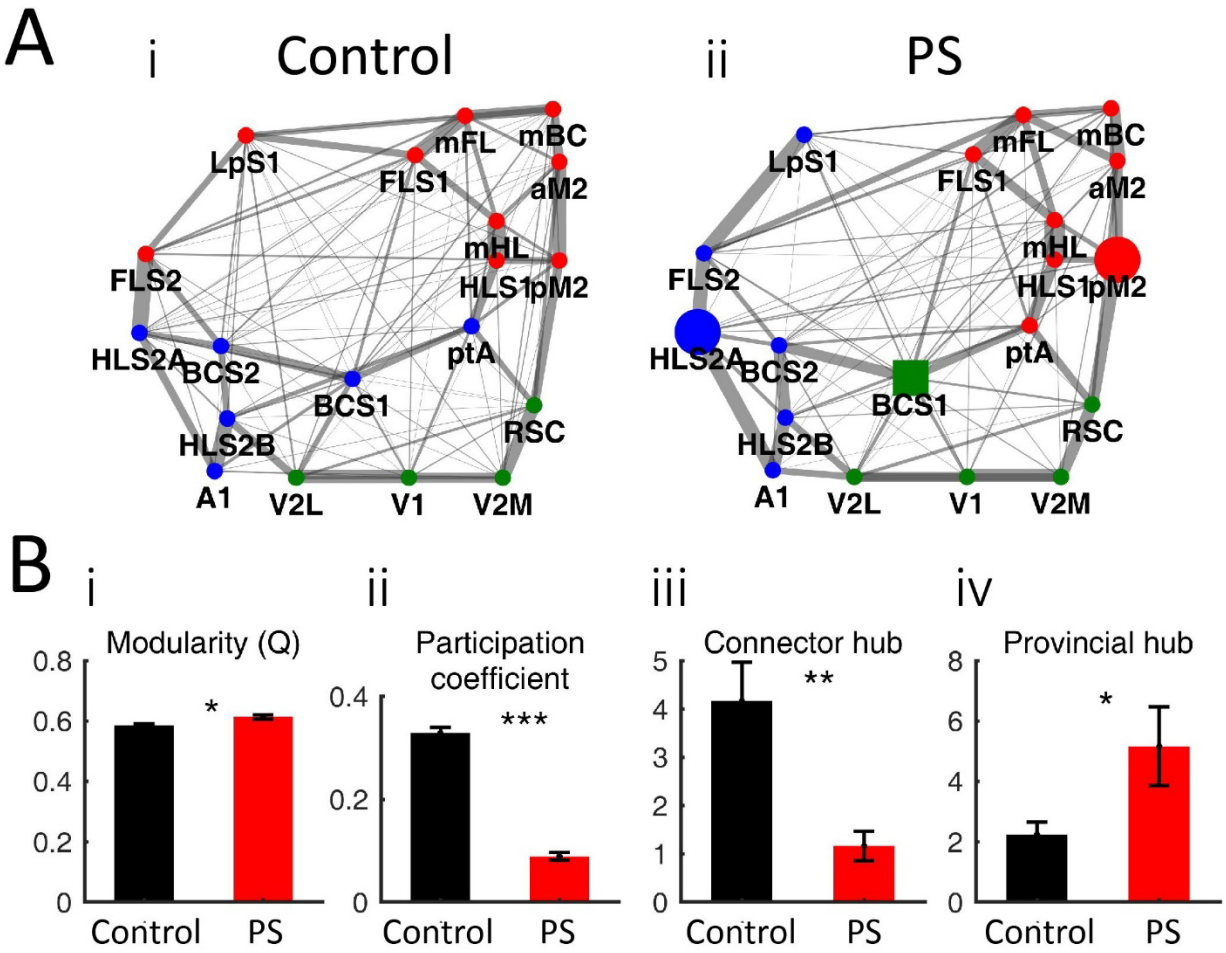

Fig 4. *PS results in delineated modules in the cortical networks*. **A**) Schematic of the cortical network based on the average partial correlation for (i) the control and (ii) PS networks. Nodes show cortical regions in the left hemisphere and edges' weight reflect the strength of the connection. The same color nodes belong to the same community. Large circles and squares represent provincial and connector hubs, respectively. **B**) Bar graphs compare network measures between the two groups. (i) The PS network showed a more modular structure as the average of its modularity quality function (Q) was greater than the control network (rank-sum=89, p=0.018). (ii) The extend of communication between regions was quantified through the participation coefficient, which was reduced in the PS compared to the control network (rank-sum=150, $p=10^{-4}$). (iii) The number of connector hubs, including high degree nodes with the participation coefficient of greater than 0.3, was greater in the control compared to the PS network (rank-sum=141.5, p=0.0065). (iv) The number of provincial hubs, consisting of high degree nodes with the participation coefficient less than 0.3, was greater in the PS than the control network (rank-sum=90, p=0.023). The bar-graphs show the average value of the measures over all animals in a group and error bars represent SEM. The number of mice: n=9 control, n=6 PS. Asterisks indicate *p<0.05, **p<0.01, or ***p<0.001. A1, primary auditory; aM2, anterior segment of the secondary motor; BCS1, primary barrel cortex; BCS2, secondary barrel cortex; FSL1, primary forelimb; FSL2, secondary forelimb; HLS1, primary hindlimb; HLS2A and HLS2B, secondary hindlimb; LpS1, primary lip; mBC, motor barrel cortex; mFL, motor forelimb; mHL, motor hindlimb; pM2, the posterior segment of the secondary motor;

PS, prenatal stress; ptA parietal association; RSC, retrosplenial cortex; SEM, standard error of mean; V1, primary visual; V2L, lateral secondary visual; V2M, medial secondary visual.

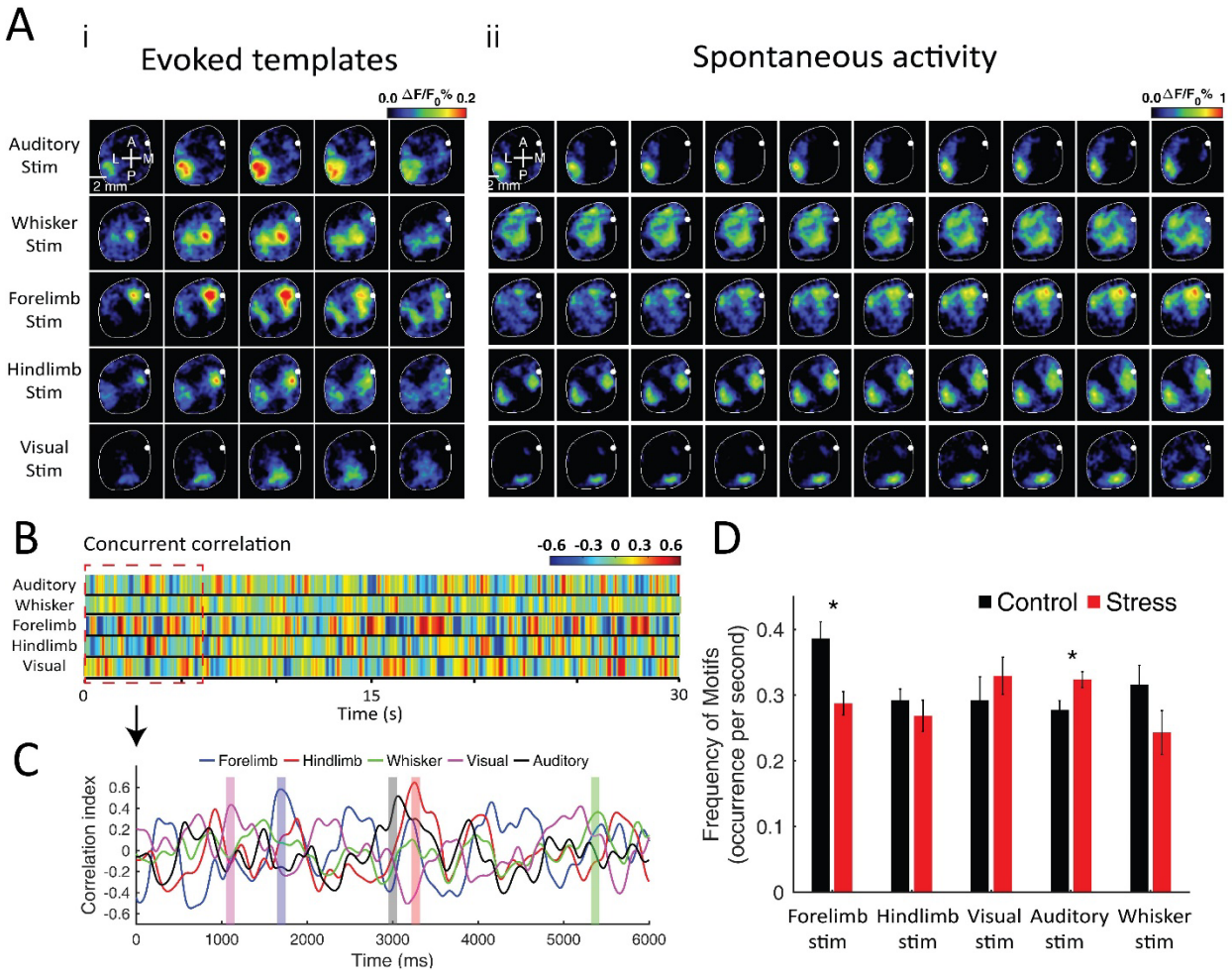

Fig 5. *Increased frequency of auditory motifs and decreased frequency of forelimb motifs in PS*. **A**) Comparison of sensory-evoked templates and spontaneous data from VSD imaging. (i) Five frames of the sensory-evoked responses to different stimuli. (ii) Spontaneous sensory motifs matched to evoked responses to auditory, whisker, forelimb, hindlimb, and visual stimuli. **B**) Concurrent correlation of different templates of sensory-evoked responses with a 30s period of spontaneous activity. The colors indicate the correlation value at different times. **C**) Correlation of sensory-evoked templates and spontaneous activity taken for 6s of spontaneous data (corresponding to the red dashed line in B). Shaded rectangles represent parts of spontaneous activity closely resembling the sensory-evoked templates, which were chosen as sensory motifs. **D**) The number of sensory motifs occurrence per second averaged over all animals in each group. The rate of occurrence in the PS group was decreased for the forelimb motif (rank-sum=27, p=0.02) and increased for the auditory motifs (rank-sum=61, p=0.04) compared with the control group. For other motifs no significant difference was observed (hindlimb: rank-sum=36, p=0.27; visual: rank-sum=51, p=0.5; whisker: rank-sum=33, p=0.142). The number of mice: n=8 control, n=6 PS.

Asterisks indicate *p<0.05, **p<0.01, or ***p<0.001. PS, prenatal stress; Stim, stimulus; VSD, voltage-sensitive dye.

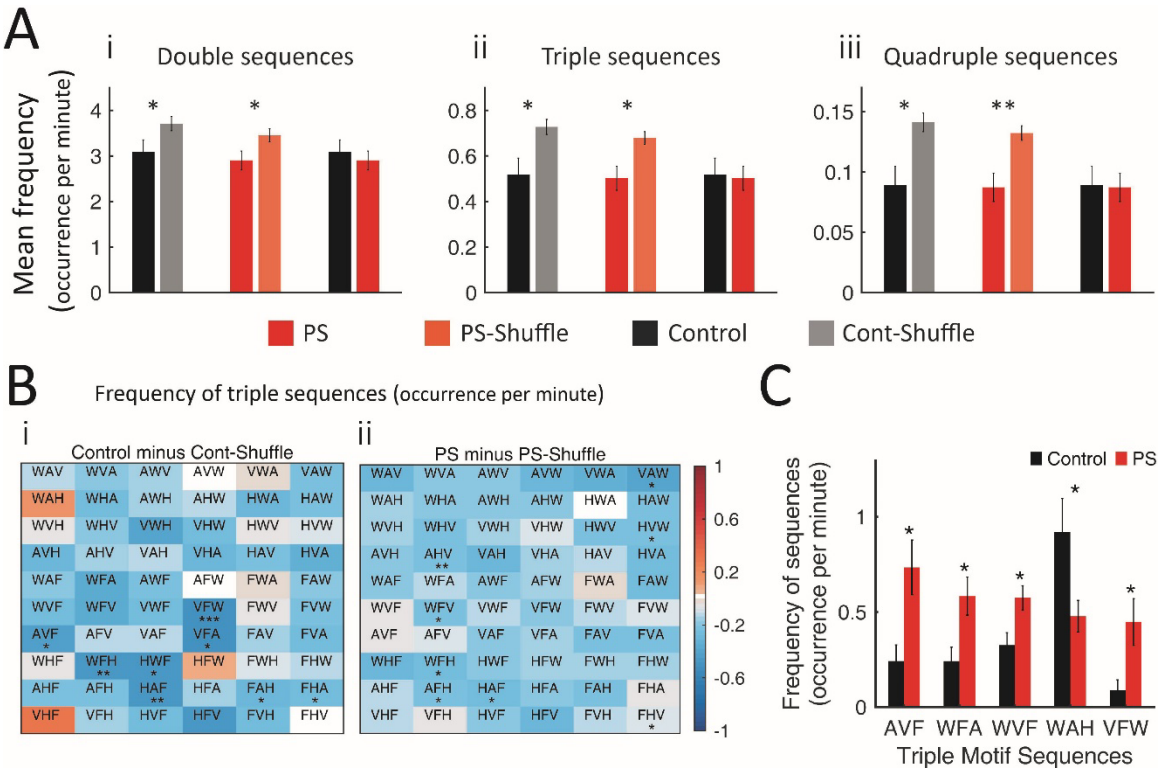

Fig 6. *Nonrandomly occurrence of sensory motifs*. **A**) Bar graphs indicate the average frequency of nonrepetitive i) double, ii) triple, and iii) quadruple sequences. Whereas, the two groups were similar in the occurrence rate of motif sequences, they significantly differ from their corresponding shuffled double, triple, and quadruple combinations (Double: Cont-Cont-Shuffle, rank-sum=49, p=0.05, Str-Str-Shuffle, rank-sum=26, p=0.04; Triple: Cont-Cont-Shuffle, rank-sum=45, p=0.012, Str-Str-Shuffle, rank-sum=23, p=0.008; Quadruple: Cont-Cont-Shuffle, rank-sum=46, p=0.02, Str-Str-Shuffle, rank-sum=21, p=0.002;). **B**) Matrices demonstrate 60 possible nonrepetitive triple motif sequences in a 10×6 block. H, F, A, W, and V stand for hindlimb, forelimb, auditory, whisker, and visual sensory motifs, respectively. The letters in each block are a short form of sequences' names, and the colors reflect changes in the occurrence rate of sequences from a random presentation. (i) In the control group, 10 cells with asterisks indicate 10 triple sequences (16%) occurred significantly different from random. (ii) In the PS group, 6 cells with asterisks imply 6 sequences (10%) occurred differently from shuffle data. **C**) Five from 60 sequences of triple combinations of motifs occurred significantly different in the two groups (AVF: rank-sum=63, p=0.02; WFA: rank-sum=63.5, p=0.015; WVF: rank-sum=63, p=0.021; WAH: rank-sum=28, p=0.03; VFW: rank-sum=64, p=0.011). The sequences not shown in this bar graph did not show a significant difference between the two groups. The number of mice: n=8 control, n=6 PS. Asterisks indicate *p<0.05, **p<0.01, or ***p<0.001. PS, prenatal stress; Cont-Shuffle, control shuffled data; PS-Shuffle, PS shuffled data.

Conflict of interest: The authors claim no conflict of interest.

Acknowledgments: The present review was supported by Canadian Institutes of Health Research (CIHR) Grant# 390930, Natural Sciences and Engineering Research Council of Canada (NSERC) Discovery Grant #40352, Alberta Innovates (CAIP Chair) Grant #43568, Alberta Alzheimer Research Program Grant # PAZ15010 and PAZ17010, and Alzheimer Society of Canada Grant# 43674 to MHM. This study was part of a postdoctoral fellowship to ZJ and a Ph.D. degree to ZR in the Canadian Center for Behavioral Neuroscience (CCBN) at the University of Lethbridge. We would like to thank Javad Karimi Abadchi for his useful comments.

6. Supplementary Methods

6.1.1. Correlation and network analysis

No threshold was introduced to the Pearson Correlation Coefficients, however, to rely on a correlation coefficient as the connection between two regions, only those with p-values less than 0.001 were kept. Specifically, as edge width distributions were significantly different in the control and PS networks (Fig. 3B), setting a threshold might give rise to biased results (Buchanan *et al.*, 2020). Note that due to the subtraction of all possible confounding correlations, the partial correlation coefficient between two regions can take negative values (Fig. S4). Note that for all network analysis we worked with weighted adjacency matrices coming from correlation analysis which included some negative values for partial Pearson correlation coefficients. Overall, all network measures were individually found for each animal and then averaged across animals for a group-level comparison.

To find out the community (modularity) structure of the networks, the community Louvain algorithm was applied (Blondel *et al.*, 2008). To adjust the size of the communities, a similar value of resolution parameter (0.2) was used for both control and PS networks. After finding the modularity structure for each animal, it was required to obtain consensus communities over all animals in each group to do a group level comparison. Hence, first, the concept of multilayer networks (Betzel *et al.*, 2019) (i.e., network layers represent individual subjects' networks) was applied. Then, the agreement matrix (Betzel *et al.*, 2013), whose

elements indicate the number of times any two vertices were assigned to the same community, was obtained. Eventually, through successively applying the Louvain algorithm on the agreement matrix (Lancichinetti and Fortunato, 2012), a consensus partition for networks of both groups was created. To define hubs, nodes that were among 80 percentile of the highest values were chosen and divided into provincial (participation coefficient<0.3) and connector (participation coefficient> 0.3) hubs (Sporns *et al.*, 2007).

6.1.2. Spontaneous sensory motifs

To determine a correlation threshold for template matching process, first, a range of thresholds was defined by summing the mean correlation between each sensory template and spontaneous activity with standard deviation (SD) in steps of 0.1 SD. Then, the number of 'matches' obtained from each threshold versus the threshold range was plotted (Supplementary Fig. 5). The threshold level was set where the percentage of 'matches' reduced to 36% (e^{-1}) of its initial value (Mohajerani *et al.*, 2013). This criterion was applied to all sensory templates individually. The overall threshold level, finally, fell around mean correlation+1.6SD for the PS group and mean correlation+1.7SD for the control group. The minimum interval between two consecutive motifs to consider them as separate events was set 200 ms.

To study the temporal order of sensory motifs within spontaneous activity, we found all possible non-repetitive combinations of motifs using the combination formula $C(n,r) = \binom{n}{r} = \frac{n!}{r!(n-r)!}$, which gives the number of possible r-combinations from a larger sample of n elements. Given five different sensory motifs, 20 double (e.g., auditory-forelimb (AF), …)., 60 triple (e.g., auditory-forelimb-visual (AFV), …)., 120 quadruple (e.g., auditory-forelimb-visual-whisker (AFVW), …)., and 120 quintuple (e.g., auditory-forelimb-visual-whisker-hindlimb (AFVWH), …) non-repetitive combinations were possible. To find these sequences, the frames of spontaneous activity matched with sensory templates were identified. Then, a combination with a certain temporal order of motifs was explored. To name a combination of motifs as a sequence, an upper limit of 1s interval between consecutive motifs was set. To verify that the order matters, the results of the experiment were compared with randomly generated sequences. To do so, the whole string of sensory motifs within a spontaneous recording was temporally shuffled (1000 times), whereas the total number of each sensory motif was kept the same as its actual count.

Legends for supplementary figures

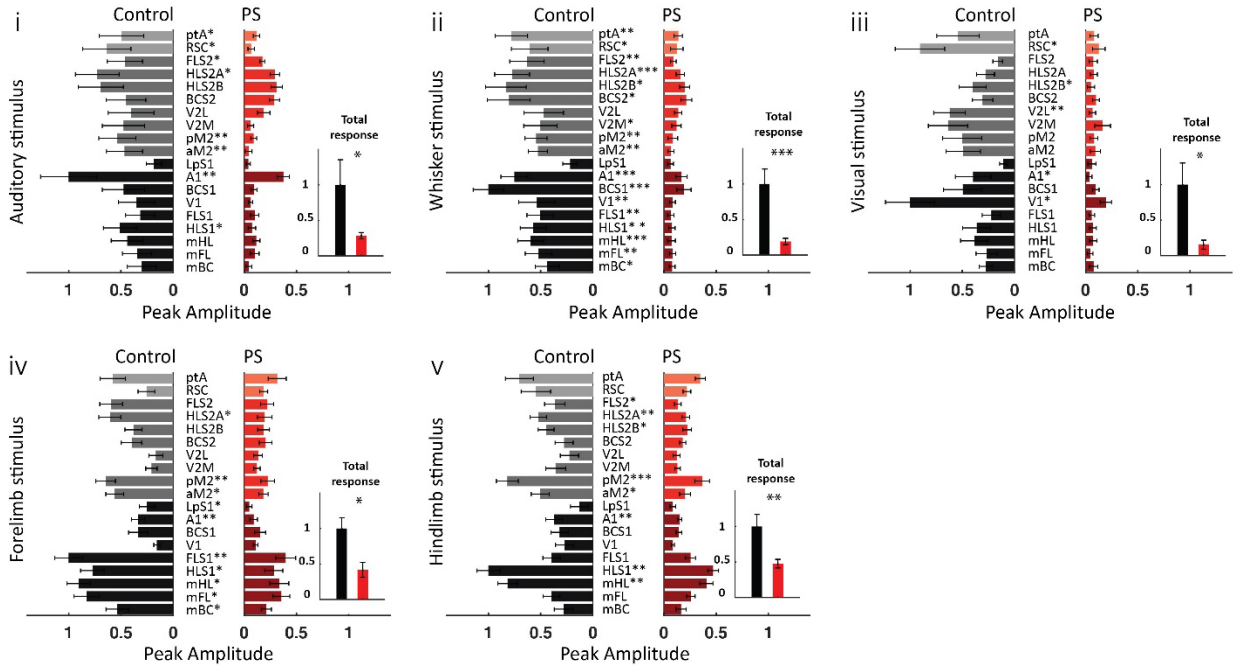

Supplementary Fig 1. *The reduced peak amplitude of evoked responses to different sensory stimuli in PS.* Peak amplitude of response to (i) auditory, (ii) whisker, (iii) visual, (iv) forelimb, and (v) hindlimb stimuli. For each stimulation, bars represent the response of each region averaged over animals per group. Note that for each stimulation, all responses (from both control and PS groups) were normalized to the largest response, which always belonged to the primary region corresponding to that sensory stimulus in the control group. Cortical regions were divided into three groups of primary sensory and motor areas (mBC, mFL, mHL, HLS1, FLS1, V1, BCS1, A1, and LPS1), supplementary areas (aM2, pMa, V2M, V2L, BCS2, HLS2A, HLS2B, FLS2), and associative areas (ptA and RSC). The gray and red spectrum colors were used for the control and PS groups, respectively. Three categories of colors in each group from dark to light indicate primary, secondary, and associative areas, respectively. Tables S3 provides related statistics. Small inset bar graphs also compare the sum of the peak amplitudes of all regions, normalized to the control group's values (auditory stimulus: $p=0.017$, rank-sum=92; whisker stimulus: $p=8\times10^{-4}$, rank-sum=98 ; forelimb stimulus: $p=0.017$, rank-sum=92 ; hindlimb: $p=0.007$, rank-sum=94 ; visual: $p=0.036$, rank-sum=90). The number of mice: n=9 control, n=6 PS. Asterisks indicate *$p<0.05$, **$p<0.01$ or ***$p<0.001$. A1, primary auditory; aM2, anterior segment of the secondary motor; BCS1, primary barrel cortex; BCS2, secondary barrel cortex; FSL1, primary forelimb; FSL2, secondary forelimb; HLS1, primary hindlimb; HLS2A and HLS2B, secondary hindlimb; LpS1, primary lip; mBC, motor barrel cortex; mFL, motor forelimb; mHL, motor hindlimb; pM2, the posterior segment of the secondary motor; PS, prenatal stress; ptA, parietal association; RSC, retrosplenial cortex; V1, primary visual; V2L, lateral secondary visual; V2M, medial secondary visual.

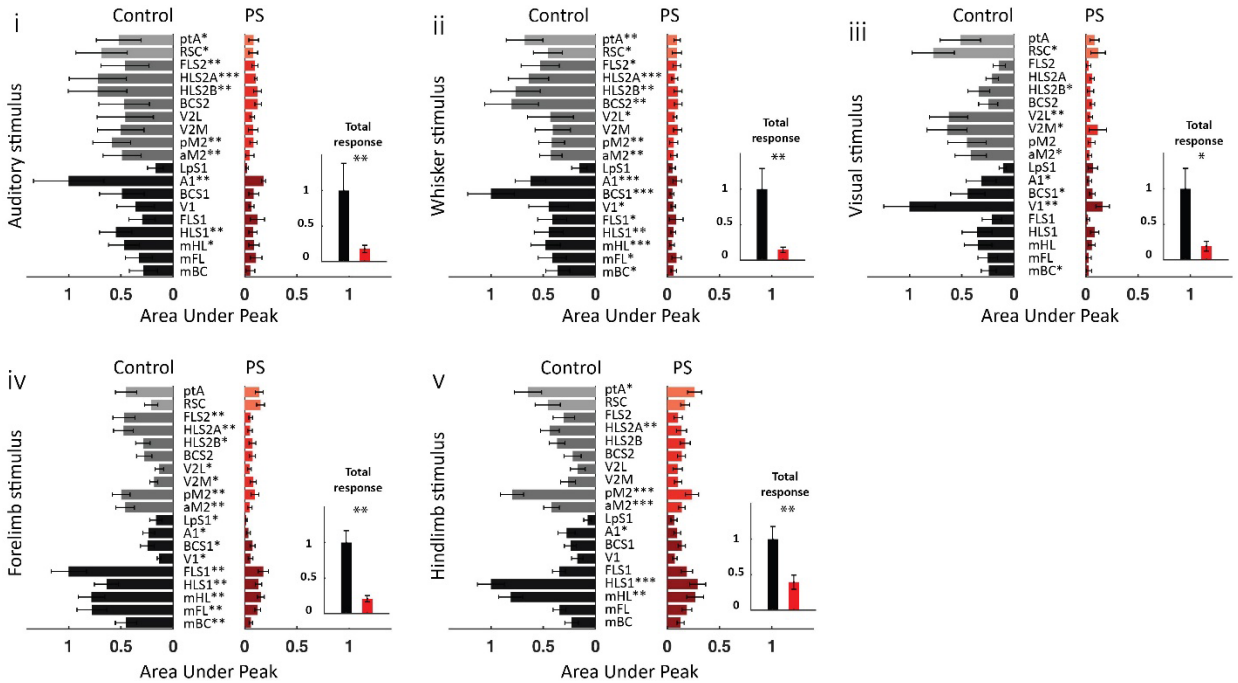

Supplementary Fig 2. *Reduced the area under the peak of the evoked responses to different sensory stimuli in PS*. Area under the peak of response to (i) auditory, (ii) whisker, (iii) visual, (iv) forelimb, and (v) hindlimb stimuli. For each stimulation, bars represent areas under the peak of the response of each region averaged over animals per group. Note that for each stimulation, all values (from both control and PS groups) were normalized to the largest one, which always belonged to the primary region corresponding to that sensory stimulus in the control group. Cortical regions were divided into three groups of primary sensory and motor areas (mBC, mFL, mHL, HLS1, FLS1, V1, BCS1, A1, and LPS1), supplementary areas (aM2, pMa, V2M, V2L, BCS2, HLS2A, HLS2B, FLS2), and associative areas (ptA and RSC). The gray and red spectrum colors were used for the control and PS groups, respectively. Three categories of colors in each group from dark to light indicate primary, secondary and associative areas, respectively. Tables S4 includes related statistics. Small inset bar graphs, also, compare sum of the area under peak of responses of all regions, normalized to the control group's values (auditory stimulus: p=0.002, rank-sum=96; whisker stimulus: p=0.004 , rank-sum=95 ; forelimb stimulus: p=0.007, rank-sum=94 ; hindlimb: p=0.004 , rank-sum=95 ; visual: p=0.017 , rank-sum=92). The number of mice: n=9 control, n=6 PS. Asterisks indicate *p<0.05, **p<0.01 or ***p<0.001. A1, primary auditory; aM2, anterior segment of the secondary motor; BCS1, primary barrel cortex; BCS2, secondary barrel cortex; FSL1, primary forelimb; FSL2, secondary forelimb; HLS1, primary hindlimb; HLS2A and HLS2B, secondary hindlimb; LpS1, primary lip; mBC, motor barrel cortex; mFL, motor forelimb; mHL, motor hindlimb; pM2, the posterior segment of the secondary motor; PS, prenatal stress; ptA, parietal association; RSC, retrosplenial cortex; V1, primary visual; V2L, lateral secondary visual; V2M, medial secondary visual.

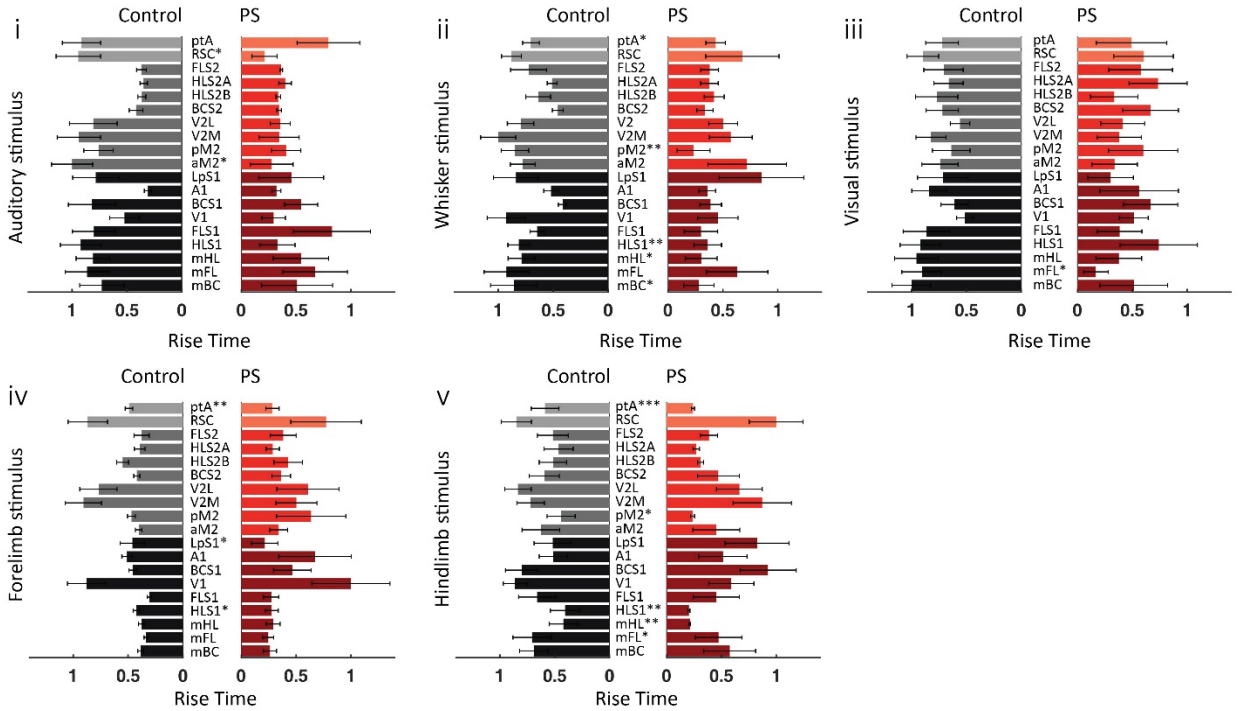

Supplementary Fig 3. *PS did not significantly affect the rise time of the peak of response to different sensory stimuli*. Rise time of response to (i) auditory, (ii) whisker, (iii) visual, (iv) forelimb, and (v) hindlimb stimuli. For each stimulation, bars represent the rise time of response of each ROI averaged over animals per group. Note that for each stimulation, all values (from both control and PS groups) were normalized to the largest rise time. Cortical regions were divided into three groups of primary sensory and motor areas (mBC, mFL, mHL, HLS1, FLS1, V1, BCS1, A1, and LPS1), supplementary areas (aM2, pMa, V2M, V2L, BCS2, HLS2A, HLS2B, FLS2), and associative areas (ptA and RSC). The gray and red spectrum colors were used for the control and PS groups, respectively. Three categories of colors in each group from dark to light indicate primary, secondary and associative areas, respectively. There were few areas for each stimulation that show a significant difference in the rise time. Tables S5 includes associated statistics. The number of mice: n=9 control, n=6 PS. Asterisks indicate *p<0.05, **p<0.01 or ***p<0.001. A1, primary auditory; aM2, anterior segment of the secondary motor; BCS1, primary barrel cortex; BCS2, secondary barrel cortex; FSL1, primary forelimb; FSL2, secondary forelimb; HLS1, primary hindlimb; HLS2A and HLS2B, secondary hindlimb; LpS1, primary lip; mBC, motor barrel cortex; mFL, motor forelimb; mHL, motor hindlimb; pM2, the posterior segment of the secondary motor; PS, prenatal stress; ptA, parietal association; ROI, region of interest; RSC, retrosplenial cortex; V1, primary visual; V2L, lateral secondary visual; V2M, medial secondary visual.

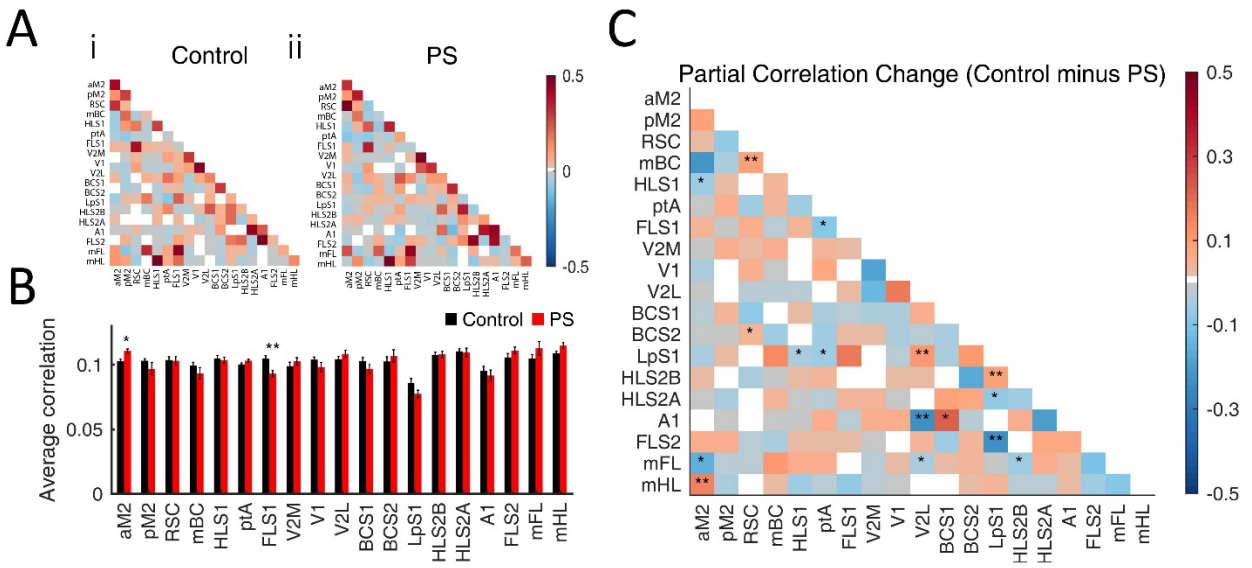

Supplementary Fig 4. *PS changed the partial correlation between a few cortical regions of interest*. **A**) Partial correlation matrices for (i) control and (ii) PS groups. **B**) The average of the partial correlation of every single region with all other regions did not show a significant difference between PS and control groups, except for aM2 (rank-sum=88, p=0.013) and FLS1 (rank-sum=142, p=0.007) regions. **C**) Subtraction of inter-regional partial correlation coefficients. The colors identify the degree of change in correlation. Whereas the inter-regional partial correlation of several areas was decreased in PS, it was increased for other areas. The alterations, however, were significant only for a few areas. The number of mice: n=9 control, n=6 PS. Asterisks indicate *p<0.05, **p<0.01 or ***p<0.001. A1, primary auditory; aM2, anterior segment of the secondary motor; BCS1, primary barrel cortex; BCS2, secondary barrel cortex; FSL1, primary forelimb; FSL2, secondary forelimb; HLS1, primary hindlimb; HLS2A and HLS2B, secondary hindlimb; LpS1, primary lip; mBC, motor barrel cortex; mFL, motor forelimb; mHL, motor hindlimb; pM2, the posterior segment of the secondary motor; PS, prenatal stress; ptA, parietal association; RSC, retrosplenial cortex; V1, primary visual; V2L, lateral secondary visual; V2M, medial secondary visual.

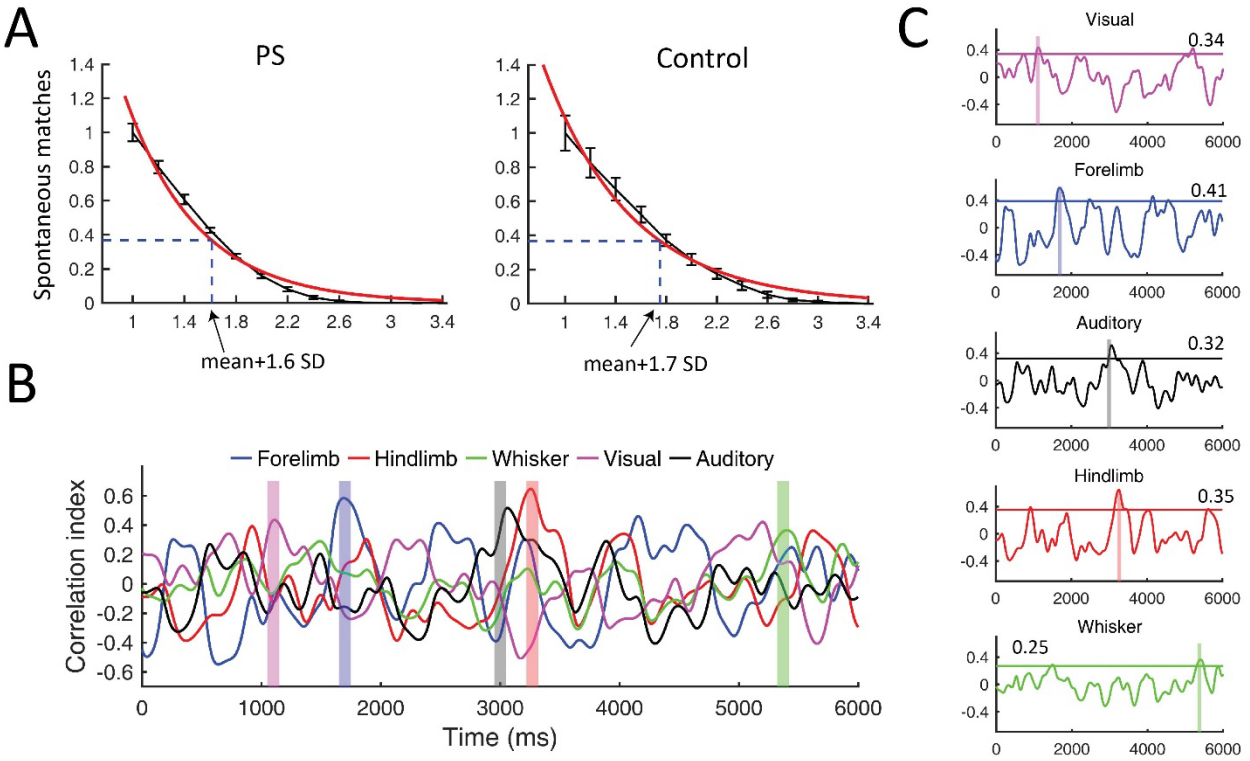

Supplementary Fig 5. *Relationship between the percentage of matched spontaneous sensory motifs and the threshold level.* **A**) The mean correlation between each sensory template and spontaneous activity was summed with standard deviation (SD) in steps of 0.1 SD to make a range of thresholds. For the forelimb sensory template, the number of 'matches' was plotted for the range of thresholds, which decreased exponentially. The threshold level was set where the percentage of matches reached 36% (e^{-1}) of its initial value. To find the e^{-1} decay, the data (black plot) was fitted with an exponential function (red plot). The intersection of the dashed line and x-axis indicates the level of threshold. Although this figure shows the threshold level for finding forelimb sensory motifs in each group, the threshold level for all other sensory motifs also fell around their mean correlation+1.6 SD for the PS group and mean correlation+1.7 SD for the control group. **B**) Correlation of sensory-evoked templates and spontaneous activity taken for 6s of spontaneous data. Shaded rectangles represent parts of spontaneous activity closely resembling the sensory-evoked templates, which were chosen as sensory motifs after meeting the threshold criterion explained in methods. **C**) The correlation plots in panel B were shown separately with their threshold levels. The threshold values were the mean correlation between each sensory template and spontaneous activity plus 1.6 SD. The number of mice: n=8 control, n=6 PS.

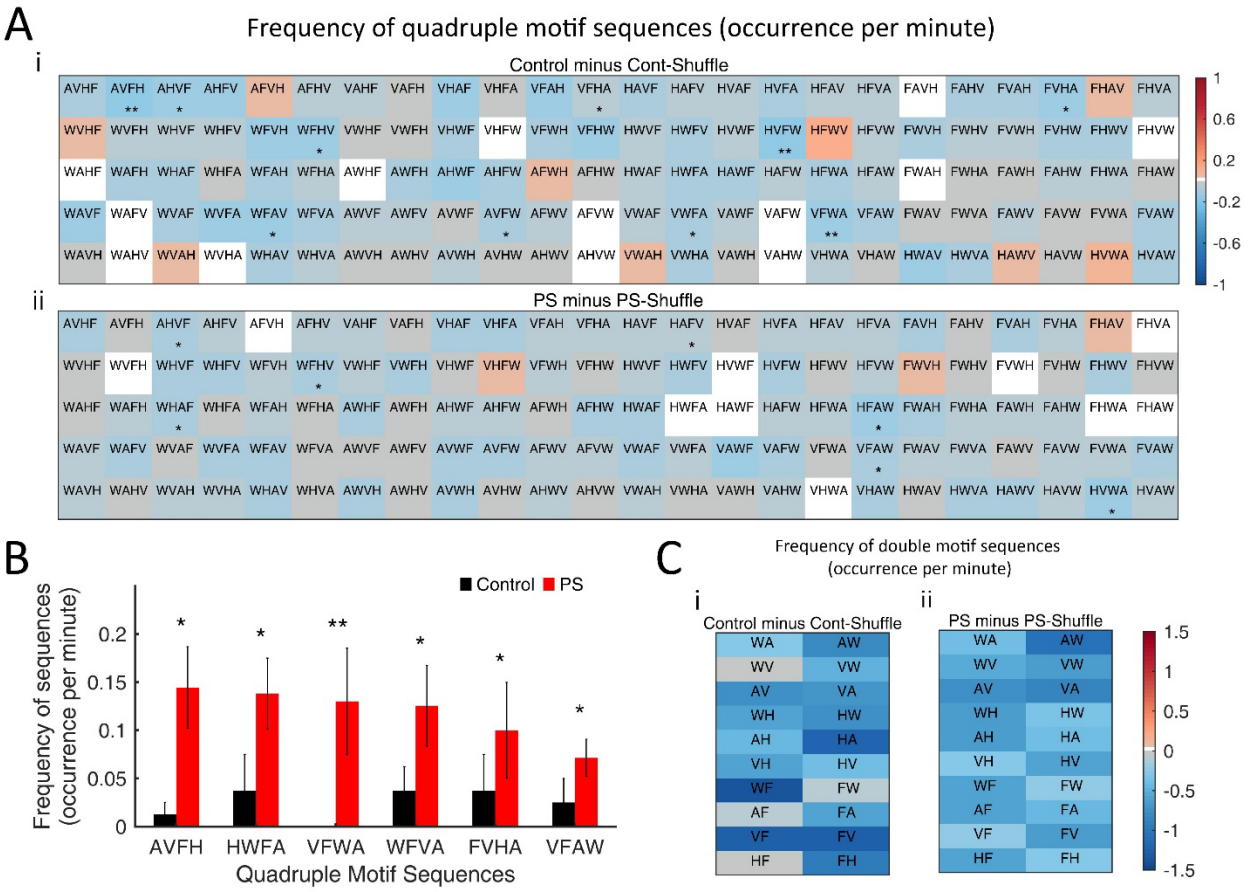

Supplementary Fig 6. *A few quadruple sequences of sensory motifs occurred more frequently in PS.* **A**) Matrices demonstrate 120 possible nonrepetitive quadruple motif sequences in a 12×5 block. H, F, A, W, and V stand for hindlimb, forelimb, auditory, whisker, and visual sensory motifs, respectively. The letters in each block are a short form of sequences' names, and the colors reflect changes in the occurrence rate of sequences from a random presentation. (i) In the control group, 10 cells with asterisks indicate 10 quadruple sequences (8%) occurred significantly different from random. (ii) In the PS group, 7 sequences (6%) occurred differently from shuffle data. **B**) 6 out of 120 double sequences of motifs (5%) occurred significantly different in the two groups (AVFH: rank-sum=63.5, p=0.011; HWFA: rank-sum=59.5, p=0.032; VFWA: rank-sum=65, p=0.006; WFVA: rank-sum=60, p=0.042; FVHA: rank-sum=60.5, p=0.027; VFAW: rank-sum=59.5, p=0.032). Other sequences not shown in this bar graph did not show a significant difference between the two groups. **C**) Matrices demonstrate 20 possible nonrepetitive double motif sequences in a 10×2 block. In both control (i) and PS (ii) groups, no sequence occurred differently from shuffle data. The number of mice: n=8 control, n=6 PS. Asterisks indicate *p<0.05, **p<0.01, or ***p<0.001. Cont-Shuffle, control shuffled data; PS, prenatal stress; PS-Shuffle, PS shuffled data.

Supplementary Table 1. Statistical parameters from the Wilcoxon rank-sum test for peak amplitude in Supplementary Fig. 1.

Brain regions	Hindlimb stimulation		Forelimb stimulation		Auditory stimulation		Whisker stimulation		Visual stimulation	
	p	rank-sum	p	rank-sum	p	rank-sum	p	rank-sum	p	rank-sum
mBC	0.607	77	0.049	89	0.093	86	0.034	90	0.053	88.5
mFL	0.388	80	0.017	92	0.106	86	0.002	97	0.075	87
mHL	0.002	96	0.012	93	0.087	87	8×10^{-4}	98	0.081	87
HLS1	0.004	95	0.012	93	0.011	93	0.002	97	0.059	88
FLS1	0.528	78	0.007	94	0.605	77	0.003	96	0.213	83
V1	0.223	83	0.688	76	0.379	80	0.007	94	0.012	92.5
BC	0.327	81	0.144	85	0.223	83	4×10^{-4}	99	0.057	88
Aud	0.002	96	0.007	94	0.004	95	8×10^{-4}	98	0.010	93
LpS1	0.286	62.5	0.019	91.5	0.092	86.5	0.062	88	0.433	79
aM2	0.012	93	0.017	92	0.003	95	0.002	97	0.059	88
pM2	8×10^{-4}	98	0.004	95	0.004	95	0.002	97	0.101	85.5
V2M	0.066	88	0.528	78	0.118	85	0.025	91	0.053	88.5
V2L	0.954	73	0.954	71	1.00	72	0.087	87	0.005	94.5
BCS2	0.954	73	0.181	84	0.688	68	0.036	90	0.256	82
HLS2B	0.025	91	0.113	86	0.066	88	0.017	92	0.018	91
HLS2A	0.004	95	0.017	92	0.025	91	4×10^{-4}	99	0.165	84
FLS2	0.025	91	0.066	88	0.025	91	0.007	94	0.213	83
RSC	0.272	82	0.711	68.5	0.037	89.5	0.011	93	0.012	92.5
ptA	0.066	88	0.223	83	0.049	89	0.004	95	0.059	88

A1, primary auditory; aM2, anterior segment of the secondary motor; BCS1, primary barrel cortex; BCS2, secondary barrel cortex; FSL1, primary forelimb; FSL2, secondary forelimb; HLS1, primary hindlimb; HLS2A and HLS2B, secondary hindlimb; LpS1, primary lip; mBC, motor barrel cortex; mFL, motor forelimb; mHL, motor hindlimb; pM2, the posterior segment of the secondary motor; ptA, parietal association; PS, prenatal stress, RSC, retrosplenial cortex; V1, primary visual; V2L, lateral secondary visual; V2M, medial secondary visual.

Supplementary Table 2. Statistical parameters from the Wilcoxon rank-sum test for the area under the peak in Supplementary Fig. S.

Brain regions	Hindlimb stimulation		Forelimb stimulation		Auditory stimulation		Whisker stimulation		Visual stimulation	
	p	rank-sum	p	rank-sum	p	rank-sum	p	rank-sum	p	rank-sum
mBC	0.388	80	0.005	95	0.125	85	0.011	93	0.229	82.5
mFL	0.113	86	0.012	93	0.106	86	0.002	96	0.149	84
mHL	0.002	97	0.007	94	0.025	91	8×10^{-4}	98	0.133	85
HLS1	8×10^{-4}	98	0.007	94	0.004	95	0.002	97	0.133	85
FLS1	0.181	84	0.005	95	0.325	81	8×10^{-4}	98	0.135	85
V1	0.181	84	0.144	85	0.213	83	0.016	92	0.008	93.5
BC	0.272	82	0.066	88	0.113	86	4×10^{-4}	99	0.022	91

Aud	0.036	90	0.004	95	0.002	97	8×10^{-4}	98	0.135	85
LpS1	0.795	74.5	0.008	93.5	0.089	86.5	0.061	88	0.954	71
aM2	4×10^{-4}	99	0.002	97	0.004	95	0.002	97	0.105	86
pM2	4×10^{-4}	99	0.005	95	0.005	95	0.003	96	0.133	84.5
V2M	0.113	86	0.144	85	0.118	85.5	0.056	89	0.007	93.5
V2L	0.688	76	0.181	84	0.270	82	0.017	92	0.003	95.5
BCS2	0.954	73	0.144	85	0.181	84	0.002	97	0.256	82
HLS2B	0.066	88	0.088	87	0.002	97	0.002	97	0.026	90
HLS2A	0.005	95	0.002	97	4×10^{-4}	99	4×10^{-4}	99	0.256	82
FLS2	0.113	86	0.007	94	0.005	95	0.002	97	1.00	72
RSC	0.272	82	0.631	76.5	0.018	91.5	0.024	91	0.027	90.5
ptA	0.025	91	0.088	87	0.025	91	8×10^{-4}	98	0.059	88

A1, primary auditory; aM2, anterior segment of the secondary motor; Aud, auditory; BC, barrel cortex; BCS1, primary barrel sensory; BCS2, secondary barrel sensory; FL, forelimb; FSL1, primary forelimb sensory; FSL2, secondary forelimb sensory; HL, hindlimb; HLS1, primary hindlimb sensory; HLS2A and HLS2B, secondary hindlimb sensory; LpS1, primary lip sensory; mBC, motor barrel cortex; mFL, motor forelimb; mHL, motor hindlimb; pM2, the posterior segment of the secondary motor; ptA, parietal association; RSC, retrosplenial cortex; SE, Standard Error; V1, primary visual; V2L, lateral secondary visual; and V2M, medial secondary visual.

Supplementary Table 3. Statistical parameters from the Wilcoxon rank-sum test for the rise time in Supplementary Fig. 3.

Brain regions	**Hindlimb stimulation**		**Forelimb stimulation**		**Auditory stimulation**		**Whisker stimulation**		**Visual stimulation**	
	p	**rank-sum**	**p**	**rank-sum**	**p**	**rank-sum**	**p**	**rank-sum**	**p**	**rank-sum**
mBC	0.272	82	0.131	85	0.341	80	0.027	90.5	0.150	84.5
mFL	0.045	89	0.063	88	0.503	78	0.288	81.5	0.018	91
mHL	0.002	97.5	0.189	83.5	0.107	86	0.013	92.5	0.133	85
HLS1	0.006	94.5	0.021	91.5	0.106	86	0.008	93.5	0.773	75
FLS1	0.061	88	0.471	78.5	0.891	73.5	0.079	87	0.179	83.5
V1	0.272	82	0.980	71.5	0.213	83	0.082	87	0.708	75.5
BC	0.863	74	0.125	85.5	0.775	75	1.00	72	0.794	69.5
Aud	0.887	73.5	0.577	77	0.712	68.5	0.173	84	0.317	81
LpS1	0.519	66	0.069	87.5	0.187	83.5	0.750	75	0.209	82.5
aM2	0.105	86	0.378	80	0.021	91	0.373	80	0.171	84
pM2	0.019	91.5	0.455	79	0.213	83	0.012	92.5	0.787	74.5
V2M	0.954	73	0.094	86.5	0.072	87.5	0.087	87	0.053	88.5
V2L	0.528	78	0.508	78	0.112	86	0.436	79	0.539	77.5
BCS2	0.170	84	0.666	76	0.476	78.5	0.443	79	0.673	76
HLS2B	0.059	88	0.181	84	0.950	73	0.547	77.5	0.191	83
HLS2A	0.060	88	0.508	78	0.435	65	0.444	79	0.622	67.5
FLS2	0.628	76.5	0.666	68	0.688	68	0.189	83.5	0.773	75
RSC	0.839	70	0.478	78.5	0.012	92.5	0.135	85	0.507	78
ptA	4×10^{-4}	99	0.004	95	0.753	75	0.047	89	0.521	78

A1, primary auditory; aM2, anterior segment of the secondary motor; Aud, auditory; BC, barrel cortex; BCS1, primary barrel sensory; BCS2, secondary barrel sensory; FL, forelimb; FSL1, primary forelimb

sensory; FSL2, secondary forelimb sensory; HL, hindlimb; HLS1, primary hindlimb sensory; HLS2A and HLS2B, secondary hindlimb sensory; LpS1, primary lip sensory; mBC, motor barrel cortex; mFL, motor forelimb; mHL, motor hindlimb; pM2, the posterior segment of the secondary motor; ptA, parietal association; RSC, retrosplenial cortex; SE, Standard Error; V1, primary visual; V2L, lateral secondary visual; and V2M, medial secondary visual.

Supplementary Table 4. Statistical parameters from the Wilcoxon rank-sum test for the bar graph in Fig. 2B.

Brain regions	p	rank-sum
aM2	0.002	145
pM2	0.009	141
RSC	0.006	142
mBC	0.004	143
HLS1	0.004	143
ptA	0.006	142
FLS1	0.009	141
V2M	0.009	141
V1	0.004	143
V2L	0.018	139
BCS1	0.004	143
BCS2	0.006	142
LpS1	0.024	138
HLS2B	0.006	142
HLS2A	0.004	143
Aud	0.001	146
FLS2	0.013	140
mFL	0.009	141
mHL	0.004	143

A1, primary auditory; aM2, anterior segment of the secondary motor; BCS1, primary barrel cortex; BCS2, secondary barrel cortex; FSL1, primary forelimb; FSL2, secondary forelimb; HLS1, primary hindlimb; HLS2A and HLS2B, secondary hindlimb; LpS1, primary lip; mBC, motor barrel cortex; mFL, motor forelimb; mHL, motor hindlimb; pM2, the posterior segment of the secondary motor; ptA, parietal association; RSC, retrosplenial cortex; V1, primary visual; V2L, lateral secondary visual; V2M, medial secondary visual.

References

Afrashteh N, Inayat S, Bermudez Contreras E, Luczak A, McNaughton B, Mohajerani M. Spatiotemporal structure of sensory-evoked and spontaneous activity revealed by mesoscale imaging in anesthetized and awake mice. BioRxiv.

Bale TL, Baram TZ, Brown AS, Goldstein JM, Insel TR, McCarthy MM*, et al.* Early life programming and neurodevelopmental disorders. Biol Psychiatry 2010; 68(4): 314-9.

Bermudez-Contreras E, Chekhov S, Sun J, Tarnowsky J, McNaughton BL, Mohajerani MH. High-performance, inexpensive setup for simultaneous multisite recording of electrophysiological signals and mesoscale voltage imaging in the mouse cortex. Neurophotonics 2018; 5(2): 025005.

Betzel R, Griffa A, Koenigsberger A, Goñi J, Thiran J, Hagmann P*, et al.* Multi-scale community organization of the human structural connectome and its relationship with resting-state functional connectivity. Network Science 2013; 1(3): 353–73.

Betzel RF, Bertolero MA, Gordon EM, Gratton C, Dosenbach NUF, Bassett DS. The community structure of functional brain networks exhibits scale-specific patterns of inter- and intra-subject variability. NeuroImage 2019; 202: 115990.

Blondel V, Guillaume J, Lambiotte R, Lefebvre E. Fast unfolding of communities in large networks. Journal of Statistical Mechanics: Theory and Experiment 2008; 2008.

Bock J, Rether K, Groger N, Xie L, Braun K. Perinatal programming of emotional brain circuits: an integrative view from systems to molecules. Front Neurosci 2014; 8: 11.

Bokil H, Andrews P, Kulkarni JE, Mehta S, Mitra PP. Chronux: a platform for analyzing neural signals. J Neurosci Methods 2010; 192(1): 146-51.

Bronson SL, Bale TL. Prenatal stress-induced increases in placental inflammation and offspring hyperactivity are male-specific and ameliorated by maternal antiinflammatory treatment. Endocrinology 2014; 155(7): 2635-46.

Buchanan CR, Bastin ME, Ritchie SJ, Liewald DC, Madole JW, Tucker-Drob EM*, et al.* The effect of network thresholding and weighting on structural brain networks in the UK Biobank. NeuroImage 2020; 211: 116443.

Bullmore E, Sporns O. Complex brain networks: graph theoretical analysis of structural and functional systems. Nature reviews Neuroscience 2009; 10(3): 186-98.

Chang TY, Beelen R, Li SF, Chen TI, Lin YJ, Bao BY*, et al.* Road traffic noise frequency and prevalent hypertension in Taichung, Taiwan: a cross-sectional study. Environ Health 2014; 13(1): 37.

Charil A, Laplante DP, Vaillancourt C, King S. Prenatal stress and brain development. Brain Res Rev 2010; 65(1): 56-79.

Clancy B, Finlay BL, Darlington RB, Anand KJ. Extrapolating brain development from experimental species to humans. Neurotoxicology 2007; 28(5): 931-7.

Crossley NA, Mechelli A, Scott J, Carletti F, Fox PT, McGuire P*, et al.* The hubs of the human connectome are generally implicated in the anatomy of brain disorders. Brain 2014; 137(Pt 8): 2382-95.

Estes ML, McAllister AK. Maternal immune activation: Implications for neuropsychiatric disorders. Science 2016; 353(6301): 772-7.

Favaro A, Tenconi E, Degortes D, Manara R, Santonastaso P. Neural correlates of prenatal stress in young women. Psychol Med 2015; 45(12): 2533-43.

Ferezou I, Deneux T. Review: How do spontaneous and sensory-evoked activities interact? Neurophotonics 2017; 4(3): 031221.

Friston KJ. Functional and effective connectivity: a review. Brain connectivity 2011; 1(1): 13-36.

Graham AM, Buss C, Rasmussen JM, Rudolph MD, Demeter DV, Gilmore JH*, et al.* Implications of newborn amygdala connectivity for fear and cognitive development at 6-months-of-age. Dev Cogn Neurosci 2016; 18: 12-25.

Grandjean J, Canella C, Anckaerts C, Ayrancı G, Bougacha S, Bienert T*, et al.* Common functional networks in the mouse brain revealed by multi-centre resting-state fMRI analysis. NeuroImage 2020; 205: 116278.

Han K, Min J, Lee M, Kang BM, Park T, Hahn J*, et al.* Neurovascular Coupling under Chronic Stress Is Modified by Altered GABAergic Interneuron Activity. The Journal of neuroscience : the official journal of the Society for Neuroscience 2019; 39(50): 10081-95.

Handa RJ, Weiser MJ. Gonadal steroid hormones and the hypothalamo-pituitary-adrenal axis. Front Neuroendocrinol 2014; 35(2): 197-220.
Heffner HE, Heffner RS. Hearing ranges of laboratory animals. J Am Assoc Lab Anim Sci 2007; 46(1): 20-2.

Hilgetag CC, Burns GA, O'Neill MA, Scannell JW, Young MP. Anatomical connectivity defines the organization of clusters of cortical areas in the macaque monkey and the cat. Philos Trans R Soc Lond B Biol Sci 2000; 355(1393): 91-110.

Huizink AC, Mulder EJ, Buitelaar JK. Prenatal stress and risk for psychopathology: specific effects or induction of general susceptibility? Psychol Bull 2004; 130(1): 115-42.

Jafari Z, Faraji J, Mirza Agha B, Metz GAS, Kolb BE, Mohajerani MH. The Adverse Effects of Auditory Stress on Mouse Uterus Receptivity and Behaviour. Scientific reports 2017; 7(1): 4720.

Jafari Z, Kolb BE, Mohajerani MH. Chronic traffic noise stress accelerates brain impairment and cognitive decline in mice. Exp Neurol 2018a; 308: 1-12.

Jafari Z, Kolb BE, Mohajerani MH. Noise exposure accelerates the risk of cognitive impairment and Alzheimer's disease: Adulthood, gestational, and prenatal mechanistic evidence from animal studies. Neurosci Biobehav Rev 2019.

Jafari Z, Mehla J, Kolb BE, Mohajerani MH. Gestational Stress Augments Postpartum β-Amyloid Pathology and Cognitive Decline in a Mouse Model of Alzheimer's Disease. Cerebral cortex (New York, NY : 1991) 2018b: 1-13.

Jensen Pena C, Monk C, Champagne FA. Epigenetic effects of prenatal stress on 11beta-hydroxysteroid dehydrogenase-2 in the placenta and fetal brain. PLoS One 2012; 7(6): e39791.

Kenet T, Bibitchkov D, Tsodyks M, Grinvald A, Arieli A. Spontaneously emerging cortical representations of visual attributes. Nature 2003; 425(6961): 954-6.

Kinney DK, Munir KM, Crowley DJ, Miller AM. Prenatal stress and risk for autism. Neurosci Biobehav Rev 2008; 32(8): 1519-32.

Kolb B, Mychasiuk R, Muhammad A, Gibb R. Brain plasticity in the developing brain. Prog Brain Res 2013; 207: 35-64.

Kolb B, Mychasiuk R, Muhammad A, Li Y, Frost DO, Gibb R. Experience and the developing prefrontal cortex. Proceedings of the National Academy of Sciences of the United States of America 2012; 109 Suppl 2: 17186-93.

Kong Y, Eippert F, Beckmann CF, Andersson J, Finsterbusch J, Buchel C*, et al.* Intrinsically organized resting state networks in the human spinal cord. Proceedings of the National Academy of Sciences of the United States of America 2014; 111(50): 18067-72.

Kyweriga M, Sun J, Wang S, Kline R, Mohajerani MH. A Large Lateral Craniotomy Procedure for Mesoscale Wide-field Optical Imaging of Brain Activity. Journal of visualized experiments : JoVE 2017(123).
Lancichinetti A, Fortunato S. Consensus clustering in complex networks. Scientific reports 2012; 2: 336.

Levenson JM, Sweatt JD. Epigenetic mechanisms in memory formation. Nature reviews Neuroscience 2005; 6(2): 108-18.

Levine S. Primary social relationships influence the development of the hypothalamic--pituitary--adrenal axis in the rat. Physiol Behav 2001; 73(3): 255-60.

Liska A, Galbusera A, Schwarz AJ, Gozzi A. Functional connectivity hubs of the mouse brain. NeuroImage 2015; 115: 281-91.

Lussier SJ, Stevens HE. Delays in GABAergic interneuron development and behavioral inhibition after prenatal stress. Dev Neurobiol 2016; 76(10): 1078-91.

Martin EA, Hlinka J, Meinke A, Dechterenko F, Tintera J, Oliver I, *et al.* Network Inference and Maximum Entropy Estimation on Information Diagrams. Scientific reports 2017; 7(1): 7062.

Maselko J, Sikander S, Bhalotra S, Bangash O, Ganga N, Mukherjee S, *et al.* Effect of an early perinatal depression intervention on long-term child development outcomes: follow-up of the Thinking Healthy Programme randomised controlled trial. Lancet Psychiatry 2015; 2(7): 609-17.

Maxwell CR, Ehrlichman RS, Liang Y, Gettes DR, Evans DL, Kanes SJ, *et al.* Corticosterone modulates auditory gating in mouse. Neuropsychopharmacology 2006; 31(5): 897-903.

McGirr A, LeDue J, Chan AW, Boyd JD, Metzak PD, Murphy TH. Stress impacts sensory variability through cortical sensory activity motifs. Transl Psychiatry 2020; 10(1): 20.

Meyer U, Murray PJ, Urwyler A, Yee BK, Schedlowski M, Feldon J. Adult behavioral and pharmacological dysfunctions following disruption of the fetal brain balance between pro-inflammatory and IL-10-mediated anti-inflammatory signaling. Mol Psychiatry 2008; 13(2): 208-21.

Mohajerani MH, Chan AW, Mohsenvand M, LeDue J, Liu R, McVea DA, *et al.* Spontaneous cortical activity alternates between motifs defined by regional axonal projections. Nat Neurosci 2013; 16(10): 1426-35.

Mohajerani MH, McVea DA, Fingas M, Murphy TH. Mirrored bilateral slow-wave cortical activity within local circuits revealed by fast bihemispheric voltage-sensitive dye imaging in anesthetized and awake mice. The Journal of neuroscience : the official journal of the Society for Neuroscience 2010; 30(10): 3745-51.

Mychasiuk R, Gibb R, Kolb B. Prenatal stress alters dendritic morphology and synaptic connectivity in the prefrontal cortex and hippocampus of developing offspring. Synapse 2012; 66(4): 308-14.

Nasiriavanaki M, Xia J, Wan H, Bauer AQ, Culver JP, Wang LV. High-resolution photoacoustic tomography of resting-state functional connectivity in the mouse brain. Proceedings of the National Academy of Sciences of the United States of America 2014; 111(1): 21-6.

Newman ME. Modularity and community structure in networks. Proceedings of the National Academy of Sciences of the United States of America 2006; 103(23): 8577-82.

Newman ME, Girvan M. Finding and evaluating community structure in networks. Phys Rev E Stat Nonlin Soft Matter Phys 2004; 69(2 Pt 2): 026113.

O'Donnell KJ, Bugge Jensen A, Freeman L, Khalife N, O'Connor TG, Glover V. Maternal prenatal anxiety and downregulation of placental 11beta-HSD2. Psychoneuroendocrinology 2012; 37(6): 818-26.

Oliver I, Hlinka J, Kopal J, Davidsen J. Quantifying the Variability in Resting-State Networks. Entropy 2019; 21(9): 882.

Pavlovska-Teglia G, Stodulski G, Svendsen L, Dalton K, Hau J. Effect of oral corticosterone administration on locomotor development of neonatal and juvenile rats. Exp Physiol 1995; 80(3): 469-75.

Paxinos G, and Franklin, KBJ. . The Mouse Brain in Stereotaxic Coordinates. San Diego: CA: Academic Press; 2001.

Power JD, Schlaggar BL, Lessov-Schlaggar CN, Petersen SE. Evidence for hubs in human functional brain networks. Neuron 2013; 79(4): 798-813.

Reynolds RM. Glucocorticoid excess and the developmental origins of disease: two decades of testing the hypothesis--2012 Curt Richter Award Winner. Psychoneuroendocrinology 2013; 38(1): 1-11.

Rubin LP. Maternal and pediatric health and disease: integrating biopsychosocial models and epigenetics. Pediatr Res 2016; 79(1-2): 127-35.

Rubinov M, Sporns O. Complex network measures of brain connectivity: uses and interpretations. NeuroImage 2010; 52(3): 1059-69.

Salas M, Schapiro S. Hormonal influences upon the maturation of the rat brain's responsiveness to sensory stimuli. Physiol Behav 1970; 5(1): 7-11.

Sapolsky RM, Romero LM, Munck AU. How do glucocorticoids influence stress responses? Integrating permissive, suppressive, stimulatory, and preparative actions. Endocr Rev 2000; 21(1): 55-89.

Scheinost D, Kwon SH, Lacadie C, Sze G, Sinha R, Constable RT*, et al.* Prenatal stress alters amygdala functional connectivity in preterm neonates. Neuroimage Clin 2016; 12: 381-8.

Scheinost D, Sinha R, Cross SN, Kwon SH, Sze G, Constable RT*, et al.* Does prenatal stress alter the developing connectome? Pediatr Res 2017; 81(1-2): 214-26.

Shoham D, Glaser DE, Arieli A, Kenet T, Wijnbergen C, Toledo Y*, et al.* Imaging cortical dynamics at high spatial and temporal resolution with novel blue voltage-sensitive dyes. Neuron 1999; 24(4): 791-802.

Spann MN, Monk C, Scheinost D, Peterson BS. Maternal Immune Activation During the Third Trimester Is Associated with Neonatal Functional Connectivity of the Salience Network and Fetal to Toddler Behavior. The Journal of neuroscience : the official journal of the Society for Neuroscience 2018; 38(11): 2877-86.

Sporns O. Towards network substrates of brain disorders. Brain 2014; 137(Pt 8): 2117-8.

Sporns O, Honey CJ, Kotter R. Identification and classification of hubs in brain networks. PLoS One 2007; 2(10): e1049.

Sporns O, Zwi JD. The small world of the cerebral cortex. Neuroinformatics 2004; 2(2): 145-62.

Thomason ME, Brown JA, Dassanayake MT, Shastri R, Marusak HA, Hernandez-Andrade E*, et al.* Intrinsic functional brain architecture derived from graph theoretical analysis in the human fetus. PLoS One 2014; 9(5): e94423.

Turesky TK, Jensen SKG, Yu X, Kumar S, Wang Y, Sliva DD*, et al.* The relationship between biological and psychosocial risk factors and resting-state functional connectivity in 2-month-old Bangladeshi infants: A feasibility and pilot study. Dev Sci 2019; 22(5): e12841.

Turkheimer FE, Leech R, Expert P, Lord LD, Vernon AC. The brain's code and its canonical computational motifs. From sensory cortex to the default mode network: A multi-scale model of brain function in health and disease. Neurosci Biobehav Rev 2015; 55: 211-22.

van den Bergh BRH, Dahnke R, Mennes M. Prenatal stress and the developing brain: Risks for neurodevelopmental disorders. Dev Psychopathol 2018; 30(3): 743-62.

Weinstock M. Prenatal stressors in rodents: Effects on behavior. Neurobiol Stress 2017; 6: 3-13.

White DR, Boettcher FA, Miles LR, Gratton MA. Effectiveness of intermittent and continuous acoustic stimulation in preventing noise-induced hearing and hair cell loss. J Acoust Soc Am 1998; 103(3): 1566-72.

Zaretsky MV, Alexander JM, Byrd W, Bawdon RE. Transfer of inflammatory cytokines across the placenta. Obstet Gynecol 2004; 103(3): 546-50.